

12-2012

## Fibulin-2 Stabilizes Tumor Extracellular Matrix And Drives Malignant Progression Of Lung Adenocarcinoma

Brandi N. Baird

Follow this and additional works at: [https://digitalcommons.library.tmc.edu/utgsbs\\_dissertations](https://digitalcommons.library.tmc.edu/utgsbs_dissertations)



Part of the [Oncology Commons](#)

---

### Recommended Citation

Baird, Brandi N., "Fibulin-2 Stabilizes Tumor Extracellular Matrix And Drives Malignant Progression Of Lung Adenocarcinoma" (2012). *Dissertations and Theses (Open Access)*. 297.  
[https://digitalcommons.library.tmc.edu/utgsbs\\_dissertations/297](https://digitalcommons.library.tmc.edu/utgsbs_dissertations/297)

This Dissertation (PhD) is brought to you for free and open access by the MD Anderson UTHealth Houston Graduate School at DigitalCommons@TMC. It has been accepted for inclusion in Dissertations and Theses (Open Access) by an authorized administrator of DigitalCommons@TMC. For more information, please contact [digcommons@library.tmc.edu](mailto:digcommons@library.tmc.edu).

**Fibulin-2 stabilizes tumor extracellular matrix and drives malignant  
progression of lung adenocarcinoma**

A

**DISSERTATION**

Presented to the Faculty of the  
University of Texas Health Center at Houston  
and

The University of Texas  
M.D. Anderson Cancer Center  
Graduate School of Biomedical Sciences

In Partial Fulfillment  
of the Requirements  
for the Degree of  
**DOCTORATE OF PHILOSOPHY**

by

**Brandi N. Baird, M.S., B.S.**

Houston, Texas

December 2012

## **ACKNOWLEDGEMENTS**

There are many individuals who have helped me tremendously over the years. I would like to thank my mentor, Dr. Kurie for his unfaltering commitment to my success and pushing me to be my best. I also appreciate my faithful committee members for having the patience to sit through my lengthy presentations and provide insight. I would also like to thank my current and previous lab mates, especially Dr. Roybal for all of his technical expertise and moral support. I would like to thank my family for their continued encouragement throughout my life and during my educational development. And most of all I would like to thank Elizabeth and her mother, Sarah, for providing love, stability, prospective, and “mental health days”. I could not have done it without any one person I have mentioned. A huge thanks to everyone for believing in the scientific potential of a small town Texas girl!

**Fibulin-2 stabilizes tumor extracellular matrix and drives malignant  
progression of lung adenocarcinoma**

Publication No. \_\_\_\_\_

Brandi N. Baird, M.S., B.S.

Supervisory Professor: Jonathan M. Kurie, M.D.

**ABSTRACT**

The ECM of epithelial carcinomas undergoes structural remodeling during periods of uncontrolled growth, creating regional heterogeneity and torsional stress. How tumors maintain ECM integrity in the face of dynamic biophysical forces is still largely unclear. This study addresses these deficiencies using mouse models of human lung adenocarcinoma. Spontaneous lung tumors were marked by disorganized basement membranes, dense collagen networks, and increased tissue stiffness. Metastasis-prone lung adenocarcinoma cells secreted fibulin-2 (Fbln2), a matrix glycoprotein involved in ECM supra-molecular assembly. Fibulin-2 depletion in tumor cells decreased the intra-tumoral abundance of matrix metalloproteinases and reduced collagen cross-linking and tumor compressive properties resulting in inhibited tumor growth and metastasis. Fbln2 deposition within intra-tumoral fibrotic bands was a predictor of poor clinical outcome in patients. Collectively, these findings support a feed-forward model in which tumor cells secrete matrix-stabilizing factors required for the assembly of ECM that preferentially favors malignant progression. To our knowledge, this is the first evidence that tumor cells directly

regulate the integrity of their surrounding matrix through the secretion of matrix-stabilizing factors such as fibulin-2. These findings open a new avenue of research into matrix assembly molecules as potential therapeutic targets in cancer patients.

## TABLE OF CONTENTS

### CHAPTER 1

Introduction.....	1
-------------------	---

### CHAPTER 2

Methods.....	5
--------------	---

<i>Animal husbandry and syngeneic tumor cell injections.....</i>	<i>5</i>
--	----------

<i>Creation of lung scaffolds and their use in an ex vivo perfusion model.....</i>	<i>6</i>
--	----------

<i>Micro-CT of devitalized lung tissue.....</i>	<i>6</i>
---	----------

<i>Mechanical Testing.....</i>	<i>6</i>
--------------------------------	----------

<i>Fractionation and LC MS/MS mass spectrometry.....</i>	<i>7</i>
--	----------

<i>Flow cytometric isolation of primary lung fibroblasts.....</i>	<i>9</i>
---	----------

<i>Sphere assays.....</i>	<i>10</i>
---------------------------	-----------

<i>Real-time quantitative PCR and ECM-specific PCR array.....</i>	<i>10</i>
---	-----------

<i>Cell adhesion assay.....</i>	<i>13</i>
---------------------------------	-----------

<i>Fibroblast matrix isolation.....</i>	<i>13</i>
---	-----------

<i>Electron microscopy.....</i>	<i>14</i>
---------------------------------	-----------

<i>Immunofluorescence.....</i>	<i>14</i>
--------------------------------	-----------

<i>Murine lung adenocarcinoma cell lines.....</i>	<i>15</i>
<i>Western blot analysis.....</i>	<i>16</i>
<i>Immunohistochemistry.....</i>	<i>16</i>
<i>Scoring of fibulin-2 expression in human lung cancers.....</i>	<i>17</i>
<i>Transfection of fibulin-2 shRNAs .....</i>	<i>18</i>
<i>Cell proliferation and anchorage independent cell growth.....</i>	<i>18</i>
<i>Invasion assays.....</i>	<i>19</i>
<i>Total and pepsin cleaved collagen content of cells in culture.....</i>	<i>19</i>
<i>Quantification of stromal collagen density.....</i>	<i>20</i>
<i>Gel zymography.....</i>	<i>20</i>
<i>Statistical Analysis.....</i>	<i>21</i>

### CHAPTER 3

<i>Results.....</i>	<i>22</i>
<i>A tumor matrix with desmoplastic reaction and infiltration by collagen-secreting CAFs.....</i>	<i>22</i>
<i>Aberrant organization of basement membranes in tumor ECM.....</i>	<i>43</i>

<i>Multi-functional role of fibulin-2 during malignant progression.....</i>	50
<i>Fibulin-2 stabilizes tumor ECM.....</i>	68
CHAPTER 4	
Discussion.....	84
GRANT SUPPORT.....	91
REFERENCES.....	92
CURRICULUM VITAE.....	100



## LIST OF ILLUSTRATIONS

FIGURE 1.....	24
<i>Collagen-rich tumor ECM.</i>	
FIGURE 2.....	26
<i>Micro-computed tomography images illustrate surface architecture of scaffolds.</i>	
FIGURE 3.....	29
<i>Strategy for global proteomic profiling of decellularized lung scaffolds.</i>	
FIGURE 4.....	36
<i>Prospective isolation strategy for LF and CAF stromal cell compartments.</i>	
FIGURE 5.....	38
<i>CAFs secrete abundant collagen type I and down-regulate collagenolytic MMP family members.</i>	
FIGURE 6.....	40
<i>CAF fibrillar collagen I secretion in vitro.</i>	
FIGURE 7.....	42
<i>CAFs induce tumor cell invasion through contact-dependent matrix secretion.</i>	
FIGURE 8.....	45

	<i>Loss of basement membrane organization within tumor ECM.</i>	
FIGURE 9.....		47
	<i>Global proteomic profiling of enriched fibroblast matrices.</i>	
FIGURE 10.....		56
	<i>Schematic illustration of CAF dependent effects on tumor-associated ECM.</i>	
FIGURE 11.....		58
	<i>Schematic illustration of proposed feed-forward model of tumor cell-derived ECM stabilizing factors which regulate matrix stabilization.</i>	
FIGURE 12.....		60
	<i>Fibulin-2 production in murine lung adenocarcinomas and normal tissue specimens.</i>	
FIGURE 13.....		63
	<i>Fibulin-2 is highly expressed in human lung adenocarcinomas and correlates with poor clinical outcome.</i>	
FIGURE 14.....		65
	<i>Derivation of fibulin-2 shRNA knock down cells in a highly metastatic KP cell line.</i>	
FIGURE 15.....		67

	<i>Fibulin-2 promotes the growth and metastatic properties of KP cells.</i>	
FIGURE 16.....		70
	<i>Fibulin-2 shRNA knock down in an additional metastatic KP cell line.</i>	
FIGURE 17.....		72
	<i>Fibulin-2 regulates diverse biological properties of tumor cells in vitro.</i>	
FIGURE 18.....		74
	<i>Representative images from in vitro proliferation and invasion assays.</i>	
FIGURE 19.....		76
	<i>Fibulin-2-deficient tumors have a reduction in fibrous stroma resulting in a less compact ECM.</i>	
FIGURE 20.....		78
	<i>Fibulin-2 regulates tensile properties, collagen solubility, basement membrane expression, and MMP remodeling enzymes.</i>	
FIGURE 21.....		81
	<i>Fibulin-2-deficient cells have reduced secretion of basement membrane components in vitro.</i>	
FIGURE 22.....		83
	<i>Schematic illustration of Fbln2-dependent effects on tumor-associated ECM.</i>	

FIGURE 23.....	86
----------------	----

*Schematic illustration of feed-forward model of tumor cell-derived fibulin-2 dependent matrix stabilization.*

## LIST OF TABLES

TABLE 1.....	12
<i>Real-time RT-PCR primer sequences.</i>	
TABLE 2.....	31
<i>ECM-related peptides up- and down-regulated in Kras<sup>LA1</sup> scaffold profiling analysis.</i>	
TABLE 3.....	33
<i>Functional classifications of ECM-related peptides up- and down-regulated in Kras<sup>LA1</sup> scaffold profiling analysis.</i>	
TABLE 4.....	49
<i>ECM-related peptides up- and down-regulated in CAF matrix profiling analysis.</i>	
TABLE 5.....	52
<i>Functional classifications of ECM-related peptides up- and down-regulated in CAF matrix profiling analysis.</i>	
TABLE 6.....	54
<i>Proteomic profiling comparison of in vivo scaffolds vs in vitro matrices analysis.</i>	

## ABBREVIATIONS

344SQ.....	mouse # 344 subcutaneous tumor
393P.....	mouse # 393 primary lung tumor
531LN2.....	mouse #531 lymph node tumor #2
7-AAD.....	7-aminoactinomycin d
Anxa1.....	annexin 1
Anxa11.....	annexin 11
Anxa3.....	annexin 2
Anxa4.....	annexin 4
APC.....	allophycocyanin
BSA.....	bovine serum albumin
CAF.....	cancer-associated fibroblast
cDNA.....	complementary DNA
Col1a1.....	collagen type 1 alpha 1
CPAS.....	Computational Proteomics Analysis System
Ctha.....	cathepsin a
Cthb.....	cathepsin b
Cthc.....	cathepsin c
Cthd.....	cathepsin d
Cthh.....	cathepsin h
DAPI.....	4',6-diamidino-2-phenylindole
DAVID.....	Database for Annotation, Visualization and Integrated Discovery
DMAB.....	dimethylaminoborane

DTT.....	dithiothreitol
ECM.....	extracellular matrix
EMT.....	epithelial to mesenchymal transition
Fbln2.....	fibulin 2
FBS.....	fetal bovine serum
FITC.....	fluorescein isothiocyanate
GFP.....	green fluorescent protein
GFR.....	growth factor reduced
GO.....	gene ontology
HRP.....	horse-radish peroxidase
HSPG2.....	heparin sulfate proteoglycan 2
IACUC.....	Institutional Animal Care and Use Committee
IPA.....	ingenuity pathway analysis
KP.....	Kras/p53
Lama3.....	laminin alpha 3
Lama5.....	laminin alpha 5
Lamb2.....	laminin beta 2
Lamc2.....	laminin gamma 2
LC/MS-MS.....	liquid chromatography-tandem mass spec
LF.....	normal lung fibroblast
LOR1.....	lysyl oxidase receptor 1
LOXL2.....	lysyl oxidase like 2
LOXL3.....	lysyl oxidase like 3

LOXL4.....	lysyl oxidase like 4
MMP-1.....	matrix metalloproteinase 1
MMP-13.....	matrix metalloproteinase 13
MMP-2.....	matrix metalloproteinase 2
MMP-8.....	matrix metalloproteinase 8
MMP-9.....	matrix metalloproteinase 9
mRNA.....	messenger RNA
PAGE.....	polyacrylamide gel electrophoresis
PBS.....	phosphate buffered saline
PCR.....	polymerase chain reaction
PE.....	phycoerythrin
PE-Cy7.....	phycoerythrin cyanine dye 7
PFA.....	paraformaldehyde
RGD.....	arginine-glycine-aspartic acid
RIPA.....	radio immunoprecipitation assay
RPMI.....	Roswell Park Memorial Institute
SDS.....	sodium dodecyl sulfate
shFbln2.....	short hairpin against fibulin 2
shRNA.....	short hairpin RNA
shSCR.....	short hairpin against scramble sequence
SPARC.....	secreted protein acid and rich in cysteine
Spna2.....	spectrin alpha 2
SYBR.....	Synergy Brands



TBST.....tris buffered saline with tween  
TEM.....transmission electron microscopy  
TGF- $\beta$ .....transforming growth factor beta  
Thy-1.....thymus cell antigen 1  
TNX.....tenascin X  
WST-1.....water-soluble disulfonated tetrazolium salt  
WT.....wild type

---

## CHAPTER 1

---

### INTRODUCTION

Epithelial tumors contain an extracellular matrix (ECM) with biophysical and biochemical features that differ sharply from those of adjacent normal tissue stroma (1). Tumor ECM is composed of a diverse array of proteins intricately oriented within a three-dimensional scaffold. These proteins include collagen fibers that serve as a structural backbone for attached glycoproteins, sulfated proteoglycans, and loosely-tethered peptide ligands (1). In response to environmental stimuli, cells secrete intrinsic matrix molecules, which integrate into and modify the surrounding scaffold through the actions of matrix cross-linking enzymes, assembly-stabilizing proteins, and proteases (2). Lysyl oxidase induces a critical step in matrix maturation through collagen cross-linking, which enhances matrix rigidity (3). Once thought to be simply a function of collagen cross-linking, tissue biomechanical properties are also modified by the deposition of proteoglycans and other ECM proteins (4). How collagen contributes to the development and progression of cancer is unclear, but malignant transformation is accompanied by dramatic increases in ECM stiffness, elevated compression forces, and high tensional resistance stresses (5). The presence of collagen-dense fibrotic foci within mammary carcinomas is correlated with adverse prognosis, and increased expression of collagen type I is associated with increased risk of metastasis in

breast, lung, and prostate cancers (6). Moreover, tumor cells migrate and invade following adherence to RGD sequences on mature matrix surfaces through integrin receptors, which are linked to an intracellular network of actin cytoskeletal and cell cortex proteins (3, 7).

Intra-tumoral matrix proteins originate from a variety of cell types, including cancer-associated fibroblasts (CAFs). In *Kras*<sup>LA1</sup> mice, which develop non-metastatic lung adenocarcinomas owing to expression of a latent, somatically activated *Kras*<sup>G12D</sup> allele (8), CAFs isolated on the basis of Thy-1 (CD90) expression exhibit sharp differences from Thy-1<sup>pos</sup> normal lung fibroblasts (LFs), including morphological and biochemical features of myofibroblasts, higher secretion of diverse cytokines and chemokines, and more potent pro-invasive effects on tumor cells (9). CAFs are thought to be largely responsible for the desmoplastic response observed in epithelial tumors characterized by a pronounced deposition of collagens, fibronectin, proteoglycans, and glycosaminoglycans (10). Another source of intrinsic matrix molecules is the tumor cell itself, and initial evidence suggests that the matrix molecules originating from tumor cells are critical for malignant progression. For example, breast cancer cells express tenascin C, which binds to membrane receptors on tumor cells that enhance the expression of stem cell factors that support metastasis-initiating ability (11). Thus, tumor cells direct matrix composition and function through secretion of key matrix molecules and recruitment of CAFs, but the matrix molecules that dictate tumor fate have not been fully defined.

To identify ECM molecules secreted by tumor cells that promote metastasis, proteomic profiling studies have been carried out on syngeneic tumor cell lines with low or high metastatic potential derived from lung adenocarcinomas which develop in mice that co-express the latent *Kras*<sup>G12D</sup> allele and a *Trp53*<sup>R172HΔG</sup> allele (designated “KP” cells and mice) (12). Numerous ECM proteins were differentially expressed, including intrinsic matrix proteins, matrix cross-linking enzymes, cell adhesion molecules, peptidases, and peptidase inhibitors (13). Of particular interest, fibulin-2 was 7.16-fold more abundant in the conditioned media of metastatic KP cells. A matrix glycoprotein and one of seven genes in the fibulin family, fibulin-2 is abundant in elastic and fibrous tissues within vessel walls and other structures (14). In cancer cells, fibulin-2 expression is quite variable, and forced expression of exogenous fibulin-2 is oncogenic or tumor suppressive in different cell types (15, 16). Although its physiological role is not clear, fibulin-2 is thought to stabilize the assembly of a variety of macromolecular structures, including tropo-elastin fibers, microfibrils, and matrix-proteoglycan complexes (17, 18). Supporting its matrix-stabilizing capacity, fibulin-2 has a carboxy-terminal globular domain and a tandem array of calcium-binding epidermal growth factor-like modules (19) and forms homodimers that fold into 3- or 4-armed structures (20). Although *Fbln2*-null mice have a normal lifespan and display no obvious defects in ECM ultrastructural features under basal conditions, myocardial infarction in *Fbln2*-null mice induces a clear phenotype of reduced cardiac tissue remodeling, attenuated TGF-β signaling within damaged cardiac tissues, and significantly improved survival (21). Collectively, these findings provide a compelling rationale to

investigate whether fibulin-2 plays a role in the development and remodeling of tumor ECM.

In this study, we sought to identify factors secreted by tumor cells that maintain ECM integrity in the face of dynamic biophysical forces that create regional heterogeneity and torsional stress. We found that Kras<sup>LA1</sup> mice and syngeneic wild-type mice injected orthotopically or subcutaneously with metastatic KP cells developed desmoplastic tumors with disorganized basement membranes owing to infiltration by collagen-secreting CAFs. KP cells secreted abundant fibulin-2, and fibulin-2 depletion disrupted the integrity of tumor ECM and inhibited tumor growth and metastasis. On the basis of findings reported here, we propose a feed-forward model in which tumor cells secrete matrix-stabilizing factors required for the assembly of an ECM that favors malignant progression.

---

## CHAPTER 2

---

### METHODS

#### Animal husbandry and syngeneic tumor cell injections

Before their initiation, all mouse experiments were submitted to and approved by the Institutional Animal Care and Use Committee at the University of Texas M.D. Anderson Cancer Center. *Kras*<sup>LA1/+</sup> and *Kras*<sup>LA1/+</sup> *p53*<sup>R172HΔg/+</sup> double mutant mice received standards of care and were euthanized according to the standards set forth by the IACUC. As previously described (22), subcutaneous tumors were generated in 129S2/SvPasCrlf mice matched on the basis of age (2 to 4 months) and gender by injection with syngeneic tumor cells ( $10^6$ ) subcutaneously into the right flank in 100  $\mu$ l phosphate-buffered saline (PBS). Mice were monitored daily for 6 weeks, at which time necropsies were performed to isolate and weigh the primary tumors and count lung metastases. Intra-thoracic (orthotopic) injections were performed as previously described (23). Briefly, 129/SV syngeneic mice matched on the basis of age (2 to 4 months) and gender were injected in the left lung lobe with 20,000 cells suspended in 50  $\mu$ l of 1:10 diluted growth-factor reduced matrigel in Hank's balanced salt solution (BD Biosciences, San Jose, CA). Mice were monitored daily for 2 weeks, at which time necropsies were performed to isolate and weigh the lung tissue and assess lymph node metastasis.

## **Creation of lung scaffolds and their use in an *ex vivo* perfusion model**

Age-matched adult rat or mouse lungs were de-cellularized using methods previously described (24). Briefly, lung tissue was harvested and native cells were removed using 1% sodium dodecyl sulfate and 1% Triton X-100 diluted in H<sub>2</sub>O in a de-cellularization chamber. Murine lung scaffolds were studied immediately or snap frozen for LC-MS/MS analysis, and rat scaffolds were used immediately for re-cellularization experiments in the *ex vivo* lung perfusion model. Briefly, 344SQ cells ( $2.5 \times 10^7$ ) were seeded through the rat lung trachea in a customized bioreactor with perfusion of oxygenated media through the pulmonary artery for 7 to 14 days (24) as described, at which point conditioned media were collected and lung lobes were formalin-fixed.

## **Micro-CT of devitalized lung tissue**

Devitalized normal or tumor burdened lungs were devitalized as previously described (24). The trachea was cannulated with a 20 gauge catheter and tied into place with a thread. Lungs (n=3, each group) were inflated with 0.5 ml of barium-sulfate contrast agent followed by micro-CT scans on a Phystech Novis small animal imaging instrument and analysis using GE Healthcare MicroView 3D Image Viewer & Analysis Tool (<http://microview.sourceforge.net/>).

## **Mechanical Testing**

For analysis of tissue compressive properties, lung disks of equal diameter were isolated by punch biopsy. Sample dimensions were measured using digital

calipers prior to compression testing (n = 4 per formulation). Compressive testing was performed using an Instron Model 3340 mounted with a 10 N load cell. Instron Series IX/s software was used for testing control, and data acquisition as uniaxial compressive strain was applied at 0.2 mm min<sup>-1</sup>. Force-elongation data was converted to stress-strain data with corrected cross-sectional area and plotted to derive the elastic modulus from the slope of the linear portion of the curve.

### **Fractionation and LC MS/MS mass spectrometry**

De-cellularized lung matrices from wild-type and Kras<sup>LA1</sup> mutant mice (4 of each type) and fibroblast matrices from LFs and CAFs (3 of each type) were prepared as described above. Following de-cellularization, the lung and fibroblast matrices were flash frozen in liquid nitrogen and stored at -80°C until subsequent processing for protein. For LC/MS-MS analysis, tumors were homogenized on liquid nitrogen and protein extracted as previously described (25). In brief, samples were lysed first in a modified RIPA buffer (PBS, pH7.4; 0.1% SDS; 0.25% Na-deoxycholate) with phosphatase and protease inhibitors at 2 ml/g, followed by further extraction of the insoluble fraction with a urea lysis buffer (PBS, pH7.4; 5.0M urea, 2.0M thiourea; 0.1% SDS; 50mM DTT). SDS and Na-deoxycholate was removed from the samples prior to fractionation with detergent removal spin columns (Pierce). Lung scaffold lysates were reciprocally labeled with either <sup>12</sup>C-acrylamide (Fluka) or <sup>13</sup>C-acrylamide (Cambridge Isotope Laboratories), combined and reduced overnight in DTT prior to fractionation on a POROS R1 10 mM column (4.6x 100mm, Applied Biosystems). Fibroblast matrix lysates were reduced



overnight in DTT prior to fractionation. Individual fractions for both sample types were trypsin digested and combined into 24 pools. Pools were then analyzed in a LTQ-ORBITRAP mass spectrometer (Thermo-Finnigan) with a nanoflow chromatography system (Eksigent). Acquired mass spectrometry data were automatically processed by the Computational Proteomics Analysis System (CPAS) pipeline using the X!Tandem search algorithm configured with the K-score module plug-in. The tandem mass spectra were searched against a mouse IPI database (v3.64) (lung scaffolds) or a composite database of IPI mouse (v3.64) and IPI bovine (v3.50) (fibroblast matrices). To estimate the significance of peptide and protein matches, we applied the tools of PeptideProphet and ProteinProphet. Peptides identified with PeptideProphet probability of a minimum 0.05 were selected and submitted to ProteinProphet; for fibroblast matrix lysates, peptides with shared bovine sequence were not included. The derived protein identifications were filtered at a maximum 5% error rate. Peptide quantitation was computed by the Q3 quantitation tool using peptides achieving PeptideProphet probability of a minimum 0.5 and fractional delta mass not exceeding 20 ppm. Enrichment analysis for Gene Ontology terms was conducted on the differentially expressed proteins by Database for Annotation, Visualization, and Integrated Discovery (DAVID;(26). GO categories with p-values >.001 and containing five or fewer genes from the list were discarded. The protein interacting networks were generated through the use of Ingenuity Pathway Analysis (IPA; Ingenuity Systems). GO terms represented in the genes from the clusters of interest were identified using DAVID.

### **Flow cytometric isolation of primary lung fibroblasts**

CAFs and LFs were isolated from the lungs of Kras<sup>LA1</sup> mice and wild-type littermates, respectively, by flow cytometric analysis to first remove hematopoietic cells (anti-CD45), endothelial cells (anti-CD31), and epithelial cells (anti-Epcam) and then positively select fibroblasts using an antibody against cell-surface glycoprotein Thy-1 (CD90) (Fig. 3A-C), which is expressed on subsets of normal lung fibroblasts and lung cancer-derived CAFs (27). Briefly, murine lungs were digested into single cell suspension by immersion in 3 mg/mL of collagenase type I (Worthington, Lakewood, NJ) and 4 mg/mL dispase II (Roche, Indianapolis, IN) and mechanical mincing on a gentleMACS Dissociator (Miltenyi Biotec, Auburn, CA) followed by gentle rocking at 37°C for 45 minutes. Dispersed cells were centrifuged, washed with PBS-2% fetal bovine serum (FBS), and subjected to red blood cell lysis (BioLegend, San Diego, CA). The remaining cells were centrifuged, washed, filtered (70 and 40  $\mu$ m) and counted (Countess, Invitrogen, Grand Island, NY) for further processing. Fibroblasts were isolated by flow cytometry using directly conjugated monoclonal rat anti-mouse antibodies against CD31, CD45, Ep-CAM, and Thy-1 and relevant isotype controls tagged with fluorochromes including FITC, PE, PE-Cy7, or APC purchased from either BD Biosciences, eBioscience (San Diego, CA), or Biolegend. 7-aminoactinomycin D (7-AAD; 2  $\mu$ g/mL, Sigma, St Louis, MO) was used as a viability dye for flow cytometric detection and exclusion of non-viable cells. Cells ( $5 \times 10^7$  cells/mL) were resuspended in PBS and 2% FBS in an optimally pre-titered cocktail of antibodies and incubated for 45 minutes on ice. The labeled cells were washed in excess PBS-2% FBS and resuspended at  $5\text{-}10 \times 10^6$

cells/mL and held on ice for flow cytometric analysis and sorting using a FACS Aria cell sorter (BD Biosciences). Fibroblasts were cultured in  $\alpha$ -modified essential medium (MEM) (Cellgro, Corning, NY) supplemented with 20% FBS, penicillin/streptomycin, L-glutamine, and sodium pyruvate. Primary cells used in experiments had been passaged fewer than 6 times.

### **Sphere assays**

Lab-Teck II eight chamber-well sterile slides were coated with Growth Factor-Reduced Matrigel (BD Biosciences). GFP-expressing 344SQ cells were seeded (900 cells per well) and cultured for 10 days or more in RPMI1640 containing 10% FBS + 0.2 % Matrigel to form spheres on the surface of the Matrigel. Fibroblasts (300 per well) were seeded on top of the established spheres, and the co-cultures were photographed at 10x after 72 hr.

### **Real-time quantitative PCR and ECM-specific PCR array**

RNA was isolated from cells using Trizol Reagent (Invitrogen), and 2  $\mu$ g of each RNA sample was reverse-transcribed using qSCRIPT (Quanta Biosciences, Gaithersburg, MD). RT-PCR analysis was performed using the ABI 7500 Fast Real-Time PCR System (Applied Biosystems) using the comparative threshold method with L32 ribosomal protein mRNA as an endogenous reference housekeeping gene. For each reaction, a standard curve was performed using serial dilutions of a mixture of cDNA samples. SYBR green I (Applied Biosystems, Foster City, CA) was used as the fluorophore. All experiments were performed in triplicate. The primer

sequences used are listed in Table 1. The RT<sup>2</sup> Profiler PCR Array, Mouse Extracellular Matrix & Adhesion Molecules (PAMM-013Z), was performed according to manufacturer's instructions (SABiosciences) using 1 µg of reverse transcribed RNA per 96-well plate with SYBR green I fluorophore detection on the ABI PCR System. Data analysis was performed using SABiosciences RT<sup>2</sup> Profiler PCR Array

Data	Software	version	3.5
------	----------	---------	-----

(<http://pcrdataanalysis.sabiosciences.com/pcr/arrayanalysis.php>).

**Table 1. Real-time RT-PCR primer sequences.**

Name	Sequence 5'-3'
m-L32 FWD	AACAGGGTGCGGAGAAGGT
m-L32 REV	TGCTCCCATAACCGATGTTG
m-Fbln2 FWD	CGCAGCTCAACACAGAGCACCG
m-Fbln2 REV	CTGTGCAATCCTGCCACGGGAC
m-LOXL3 FWD	GGAACAGTCTGTGACCGAAAGTG
m-LOXL3 REV	CACTCAAGTGGATGGCACCCAT
m-LOXL4 FWD	TTCTCGGCTGGCGTTGCTTGTA
m-LOXL4 REV	GGAATTGGAGAGGCAGTTTTCC
m-MMP-2 FWD	TGGGGGAGATTCTCACTTTG
m-MMP-2-REV	ACTTGTCTTCTCCCAGGGT
m-MMP-7 FWD	GAGTGCCAGATGTTGCAGAA
m-MMP-7 REV	CTGGAATGCCATTTTGGACT
m-MMP-9 FWD	CCAGACGTGGGTTCGATTCC
m-MMP-9 REV	ATGATGGTCCCACCTTGAGGC
m-Fn1 FWD	GACCGGGGACTCACATCCA
m-Fn1 REV	AGATTGATAGGGAACCTCGTCCA
m-Col4a1 FWD	TATTGAGTCACCTCTCGTGAACA
m-Col4a1 REV	TGGCTGTCTTAGGCTAATGGG
m-Lama2 FWD	GTATGGTCTTGAAAATACAAC
m-Lama2 REV	GATTCTGCTCTGGAGTTGGTCC
m-Lama5 FWD	CACCGAAGTGGTCTATTCTGGC
m-Lama5 REV	CCTACGCTTACATTGACACTCC
m-Lamb1 FWD	GTACATTGGCTCCAGATGTGATGACT
m-Lamb1 REV	GGCAATGGTCCCCTTCTGTGTGGT
m-Lamb2 FWD	AGAAGGCAGAGACAGTCCAAGC
m-Lamb2 REV	GTATTGGTCACCTACTTGTTCC
m-Lamc1 FWD	GTGTGAACGATAACAAGACAGC
m-Lamc1 REV	CATACCGTTACCTCATTATCC
m-Lamc2 FWD	TCGTATCAGCACAGTCTCCG
m-Lamc2 REV	GCAACCTTCTGGCTAATAGAGG
m-HSPG2 FWD	GGAGAGTCCTCCATATGCCA
m-HSPG2 REV	GGATGGAAGTGTCAGGGAGA

### **Cell adhesion assay**

Cells were harvested through trypsinization and resuspended as triplicates in serum containing medium at  $5 \times 10^4$  cells/ml into a 24-well plate. Plates were incubated at 37°C for 1, 2, and 3 hour time points. The wells were washed with PBS to remove non-adhering cells and remaining cells were fixed and stained with 0.1% crystal violet. The crystal violet dye was solubilized with 10% acetic acid and transferred into 96-well plates to measure optical density at 595 nm. Cell adhesion on different ECM substrates was examined based on a modification of a protocol (28) in which 96-well plates were pre-coated in triplicate with 5  $\mu\text{g}/\text{cm}^2$  of corresponding ECM protein overnight at 4°C. Wells were washed with PBS and blocked with 0.5% BSA for 1 hour at room temp. Cells were serum-starved for 1 hour prior to attachment assay at which point they were trypsinized and resuspended in serum free media at  $5 \times 10^4$  cells/mL. Cell suspensions (100  $\mu\text{l}$ ) were added to each well. Cells were allowed to adhere for 1 hour at 37°C followed by fixation and staining with 0.1% crystal violet, which was solubilized in 10% acetic acid, and quantified at 595 nm wavelength. Results were expressed as mean values  $\pm$  SD from triplicate wells.

### **Fibroblast matrix isolation**

CAF and LF extracellular matrices were isolated based on a modification of previously published methods (29). Briefly, fibroblast mono-cultures were grown to confluence in 150 mm plates in  $\alpha$ -modified essential medium (Sigma Aldrich) supplemented with 20% FBS, penicillin/streptomycin, 1X L-glutamine, and 1X

sodium pyruvate. To enhance matrix secretion, L-ascorbic acid (50 µg/ml) was freshly prepared and added at each media change. For matrix isolation, cells were lysed in water for 10 minutes at which point cellular debris was removed. The remaining matrices (n=3, each group) were scraped from plates and snap frozen for later mass spec analysis or tumor sphere assays in Matrigel cultures.

### **Electron microscopy**

Transmission electron microscopy (TEM) was performed on glutaraldehyde-fixed, plastic embedded tissue. The basement membrane along with other ECM features was assessed at ultrastructural level. Ultrastructural examination allowed for assessment of the lamina rara and lamina densa of the basement membrane. The basement membrane was evaluated for intactness, discontinuity, and irregular architecture, as well as measurement of the thickness of the basement membrane and its components (lamina rara and lamina densa). In addition, both qualitative and quantitative assessment of elastic fibers, interstitial collagen fibers, and extracellular matrix ground substance making up the intertidal compartment were determined. The ultrastructural characteristics and thickness of the interstitial component of the samples were assessed both qualitatively and quantitatively. The quantitative measurements were made using software integrated within the transmission electron microscope software programs currently available.

### **Immunofluorescence**

Five  $\mu\text{m}$  adult mouse sections were derived as described above. Slides were rehydrated and incubated in blocking buffer (5% BSA, 1% Skim Milk, 0.05% Triton X-100 in PBS) for 1 hour at room temperature. Sections were incubated overnight with antibodies against collagen IV (Abcam) then washed in PBS (0.05% Tween 20) and incubated with donkey anti-rabbit-FITC (Jackson ImmunoResearch, West Grove, PA) for 1 hour at room temp and then rinsed. Sections were cover-slipped in Pro-Long Gold anti-fade mounting media containing DAPI (Sigma Aldrich, St. Louis, MO). Photomicrographic images were acquired using an Olympus IX71 inverted fluorescent microscope. Images were colored and overlaid using Olympus DP Manager software version 2.1.1.163. For chamber slide immunofluorescence, cells were cultured to confluence on 8 well glass Lab-Tek chamber slides (Thermo Scientific) and fixed in 1% PFA for 30 minutes followed by blocking with serum-free protein block (DAKO) for 1 hour. Chamber slides were stained for one hour at room temperature with polyclonal rabbit antibodies against collagen type I (Abcam), collagen type IV (Abcam), or laminin (Abcam) and rinsed in PBS (0.05% Tween 20). Sections were incubated with donkey anti-rabbit Alexa 594 (Invitrogen). Chamber wells were removed and slides were cover-slipped in Pro-Long Gold anti-fade mounting media containing DAPI.

### **Murine lung adenocarcinoma cell lines**

All murine adenocarcinoma cell lines used in this study were previously derived from spontaneously occurring tumors in mice harboring both the *K-ras*<sup>G12D</sup> and *p53*<sup>R172H $\Delta$ G/+</sup> genetic mutations (12). Cell lines were named according to the



mouse number and site of derivation (e.g., 393P, denotes primary lung tumor; 344SQ, subcutaneous metastasis). These cells have alveolar type II cell properties and variable propensities to undergo EMT and metastasize following injection into syngeneic mice (22).

### **Western blot analysis**

Lysates from cell lines were harvested using RIPA buffer and were separated by SDS-PAGE and transferred onto a polyvinylidene fluoride nitrocellulose membrane (Bio-Rad Laboratories, Hercules, CA). Membranes were blocked overnight at 4°C in TBST with 5% nonfat dry milk followed by incubation with primary antibodies against fibulin-2 (Abcam, Cambridge, MA) and beta actin as an internal control in TBST with 2.5% nonfat dry milk overnight at 4°C. Secondary antibodies linked to HRP were incubated for 1 hour at room temperature followed by detection with an enhanced chemiluminescence kit according to the manufacturer's instructions (Amersham, Pittsburgh, PA). Band intensities were quantified based on densitometry using Image J Software (<http://rsbweb.nih.gov/ij/>).

### **Immunohistochemistry**

Mouse and human tissue specimens were fixed in 10% formalin and embedded in paraffin. Five µm paraffin sections were de-paraffinized with xylene and rehydrated in ethanol washes followed by incubation in antigen retrieval solution (DAKO, Carpinteria, CA) for 20 mins at 95°C followed by rinsing and blocking of endogenous peroxidase with 3% H<sub>2</sub>O<sub>2</sub> in cold methanol for 20 minutes.

Slides were rinsed and incubated in blocking buffer (5% BSA, 1% Skim Milk, 0.05% Triton X-100 in PBS) for 1 hour at room temperature. Sections were then incubated overnight in a humidified chamber with antibodies against fibulin-2 (Novus Biologicals) at 1:250 dilution then washed in PBS (0.05% Tween 20) and incubated with donkey anti-rabbit-HRP (Jackson ImmunoResearch) diluted 1:500 for 1 hour at room temp and then rinsed and developed 3 to 5 minutes in liquid DAB substrate solution (DAKO). Slides were rinsed in H<sub>2</sub>O and counter stained with Meyer's hematoxylin, dehydrated, and cover-slipped in xylene-based mounting medium. Photomicrographic images were acquired using an Olympus IX71 inverted fluorescent microscope.

### **Scoring of fibulin-2 expression in human lung cancers.**

Immunohistochemical studies were carried out on tumor tissue specimens obtained from 46 surgically resected human lung adenocarcinomas, stages I-III, resected with curative intent. All cases were fully annotated for demographic variables, pathologic stage, smoking status and clinical outcome. Fibrillar and fibrous fibulin-2 staining was quantified separately in tumor, adjacent normal lung parenchyma, and lung tissue scars. The distribution of fibulin-2 expression was quantified in the peripheral areas (defined as the ~25% peripheral portion of the tumors) and central areas (defined as the ~75% central portion of the tumors). Scoring was performed by an experienced lung cancer pathologist (I.W.) using the percentage (0-100%) of the extent of reactivity. For analysis, the pattern of distribution of tumor scores was characterized (Gaussian, bimodal, etc.). The data

were analyzed as continuous variables and as dichotomous variables (high *versus* low, using median value as a cut point). For each tumor, the final score was the intensity value multiplied by reactivity extension value (range, 0-300) as previously reported (30).

### **Transfection of fibulin-2 short hairpin RNAs (shRNAs)**

We sub-cloned murine *Fbln2*-specific shRNAs (Sigma-Aldrich) and scrambled shRNA (Addgene, plasmid 1864) into lentiviral pLKO.1 TRC (Addgene, Plasmid 10878). Additionally, pGIPZ lentiviral vectors containing *Fbln2*-specific shRNA sequences (V3LMM\_515480 & V2LMM\_26531) were purchased (Open Biosystems, Lafayette, CO). The target sequences for murine fibulin-2 were as follows: shFIBULIN-2#1, GGAGCAGAGGACAATGATA; shFIBULIN-2#2, GCACTACCAGCTCAATTTC; shFIBULIN-2#3, CCACTGTGTTCTCAATTA; and shFIBULIN-2#4, CGTCTCACTCTACAAGCAA. These vectors were packaged in 293T cells by co-transfection with packaging vectors psPAX2 (Addgene, Plasmid 12260) and pMD2.G (Addgene, Plasmid 12259). Cells (344SQ and 531LN2) were infected with viral particles and selected in puromycin (10 µg/ml) for up to 14 days to generate stable transfectants.

### **Cell proliferation and anchorage independent cell growth**

For cell proliferation assay cells were harvested by trypsinization and seeded at serial dilution concentrations of 1, 10, 100, and 1000 cells in 96-well plates. WST-1 assay was carried out at 24, 48, and 72 hours per manufacturer's instructions

(Millipore, Billerica, MA) with colorimetric readings taken at 440 nm. Results were expressed as mean values  $\pm$  SD from triplicate wells. For anchorage independent cell growth cells ( $5 \times 10^4$  in 0.3% agar) were seeded onto a layer of 0.8% agar in 6-well plates, allowed to proliferate for 21 days, and stained with crystal violet. Colonies were visualized by light microscopy and scored per field of view. Results were expressed as mean values  $\pm$  SD from triplicate wells.

### **Invasion assays**

As described previously (9), cells in serum-free RPMI 1640 ( $5 \times 10^4$ ) were seeded onto Transwell plates coated with GFR-Matrigel (BD Biosciences), with RPMI 1640/10% FBS in the lower well as the chemo-attractant. Each condition was performed in triplicate or quadruplicate. After 16–18 h of incubation, the medium was removed and the cells were fixed with 90% ethanol. The migrated cells were fixed and stained with 0.1% crystal violet, which was solubilized in 10% acetic acid, and quantified at 595 nm wavelength. Results were expressed as mean values  $\pm$  SD from triplicate wells.

### **Total and pepsin cleaved collagen content of cells in culture**

Hydroxyproline measurements of total collagen were conducted according to manufacturer's instructions (Cedar Lane Laboratories, Burlington, NC). Briefly, equal cell densities were plated and allowed to reach confluence for enhanced collagen deposition. Cell homogenates were isolated in equal volumes of H<sub>2</sub>O and diluted to a final concentration of 6N HCL. Samples were hydrolyzed by baking at

110°C for 24 hours at which point floating lipid was removed and samples were evaporated using speed vacuum without heat and resuspend in equal volumes of H<sub>2</sub>O for subsequent oxidation with chloramine-T and quantification using DMAB substrate at 560 nm. Sircol measurements of solubilized collagen were performed according to manufacturer's instructions (Biocolor, Carrickfergus, UK) on 4°C overnight pepsin digested cell extracts (1 mg/mL gastric pepsin) producing solubilized collagen fragments detected by Picosirius red substrate and acid-salt wash followed by quantification at 555 nm.

### **Quantification of stromal collagen density**

Tissue sections of fibulin-2-deficient and –replete flank tumors were stained with Picosirius red according to manufacturer's instructions (Polysciences, Warrington, PA). Stained tumor sections were converted into binary images using Image J software (<http://rsbweb.nih.gov/ij/index.html>). “Particles” defined as fully enclosed areas within the binary images were counted in 48 defined areas (grids) within the interior of the tumor, excluding subcutaneous fascia, and the surface area of each particle was measured.

### **Gel zymography**

MMP2 and MMP9 enzymatic activities were measured by gelatin zymography, as previously described by BioRad (Hercules, CA). The gelatin in the gel was digested by MMP activities and was visualized as a clear band on a coomassie blue-stained background. Quantitation of the MMP band was performed

by the Quantity One Gel Documentation System (Bio-Rad Laboratories, Hercules, CA, USA). Total protein stained with coomassie blue served as a normalization control.

### **Statistical Analysis**

Numerical values of mouse cohort data were analyzed using student's t-test for significance in GraphPad software. The difference was considered significant at  $P < 0.05$  (two-tailed). Summary statistics for human data were provided to describe patient characteristics and Fibulin-2 expression. The clinical end points were overall survival time and time-to-recurrence. Repeated measures analysis using mixed model was employed to assess the difference in fibulin-2 expression between intra-tumoral locations. Overall survival duration and time-to-recurrence were estimated using the Kaplan-Meier method. Comparisons between and among patient demographic groups were assessed using log-rank test. Univariate Cox proportional hazard model was applied to assess the effect of covariates and fibulin-2 expression on overall survival time and time-to-recurrence. All computations were carried out in SAS 9.2 and S-plus 8.0.

---

## CHAPTER 3

---

### RESULTS

#### **A tumor matrix with desmoplastic reaction and infiltration by collagen-secreting CAFs**

To investigate ECM changes that accompany lung tumorigenesis, lungs from syngeneic wild-type and Kras<sup>LA1</sup> mice were devitalized to generate purified tissue matrices (termed Kras<sup>WT</sup> and Kras<sup>LA1</sup> scaffolds, respectively). On gross inspection, dense ECM deposits were apparent within devitalized lung tumors in Kras<sup>LA1</sup> scaffolds, whereas Kras<sup>WT</sup> scaffolds had a homogeneous appearance (Fig. 1A). Micro-computed tomographic imaging following airway inflation revealed that Kras<sup>LA1</sup> scaffolds had loss of the dimpled surface appearance of Kras<sup>WT</sup> scaffolds (Fig. 2). There were numerous dense collagen bundles within devitalized lung tumors as evidenced by Masson's trichrome staining (Fig. 1B). Transmission electron microscopic analysis demonstrated an increased proportion and thickness of collagen bundles within devitalized lung tumors (Fig. 1C). In light of the collagen enrichment of Kras<sup>LA1</sup> scaffolds, we examined the stiffness of non-devitalized lung tumors relative to that of normal lung tissues using a mechanical testing device that measures the bulk compressive properties of tissue punches irrespective of sample geometry. Tumors from Kras<sup>LA1</sup> mice had greater stiffness than did normal lungs from wild-type littermates (Fig. 1D).

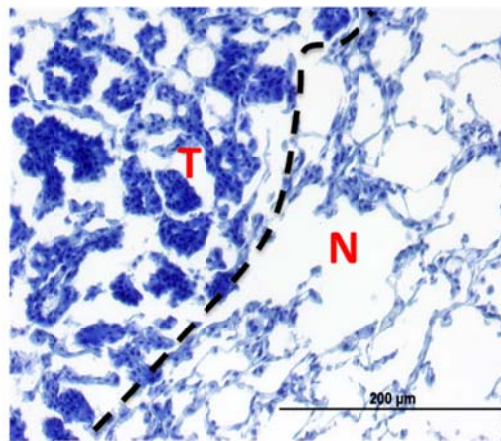
**Figure 1. Collagen-rich tumor ECM.** (A) ECM scaffolds were created by detergent-based de-cellularization of whole lungs isolated from  $Kras^{LA1}$  mice and wild-type mice.  $Kras^{WT}$  scaffolds have a homogeneous appearance (A, left panel) whereas  $Kras^{LA1}$  scaffolds have areas of hyperdense stroma (arrow) in tumoral regions (A, right panel). (B, C) Dense collagen bundles in tumoral regions of  $Kras^{LA1}$  scaffolds by Masson's tri-chrome stain (B) and transmission electron microscopy (C, right panel) were absent in  $Kras^{WT}$  scaffolds (C, left panel). T, tumor; N, normal lung. (D) Compressive moduli of punch biopsies from normal lung (n=13) and lung tumors (n=9) were measured using a mechanical testing device. Scatter plot representation of compressive modulus in each tissue sample (squares), mean values in each cohort (long line), and standard deviations (short line). P-values are indicated (t-test).



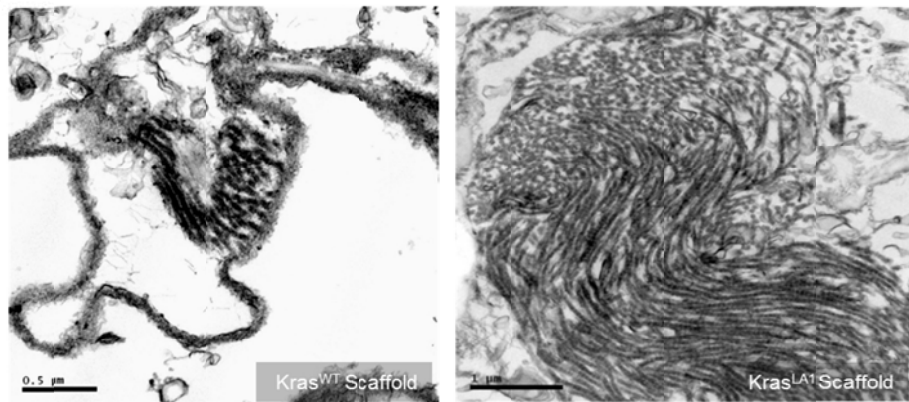
A



B



C



D

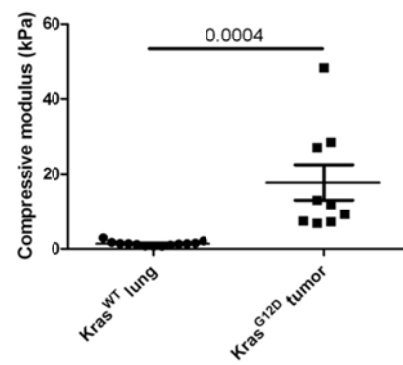
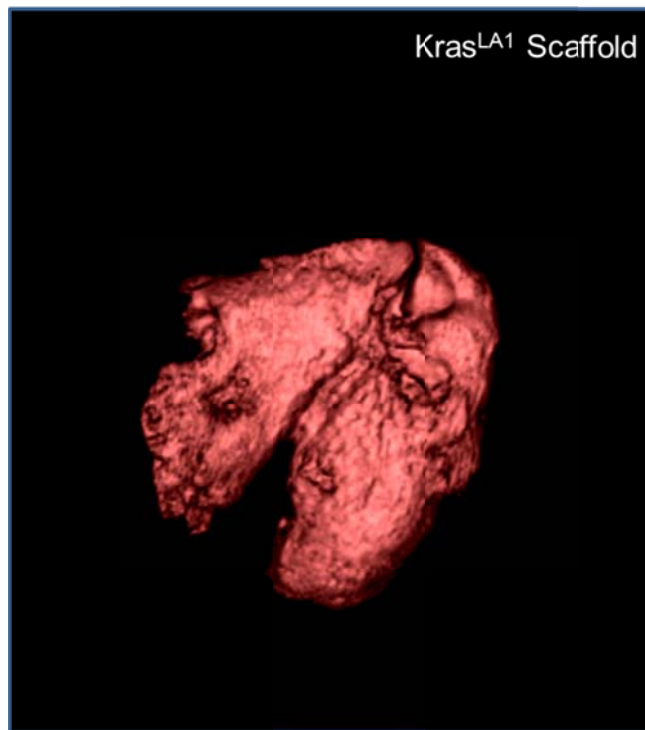
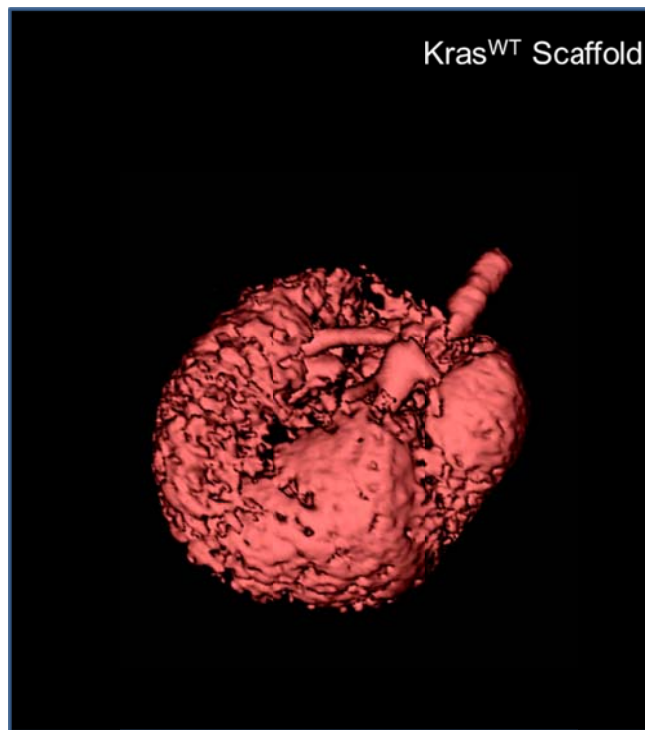


Figure 1

**Figure 2.** *Micro-computed tomography images illustrate surface architecture of scaffolds.* Dimpled surface architecture of Kras<sup>WT</sup> scaffolds (top panel) is attenuated in Kras<sup>LA1</sup> scaffolds (bottom panel).



**Figure 2**

To investigate ECM composition of the devitalized lungs, liquid chromatography-mass spectrometry (LC-MS/MS) analysis was performed on scaffold protein extracts following reciprocal acrylamide labeling of cysteine residues (schema diagrammatically illustrated in Fig. 3A). Quantification of spectra from Kras<sup>WT</sup> and Kras<sup>LA1</sup> scaffolds demonstrated up- or down-regulation of 211 proteins ( $> 1.5$ -fold,  $P < 0.05$ , same trend with reverse labeling, Table 2) that were enriched in multiple Gene Ontology terms, including “carbohydrate catabolism” ( $p=1.7E-06$ ), “mitochondrion” ( $p=9.32E-06$ ), and “glucose catabolism” ( $p=1.98E-04$ ) (Fig. 3B). Kras<sup>LA1</sup> scaffolds were enriched in multiple ECM peptides, including collagen type I  $\alpha 1$  (2.03-fold), fibronectin (1.56-fold), SPARC (2.11-fold) and tenascin X (2.36-fold) (Table 3). A number of cleaved forms of cathepsin family members were up-regulated, including Ctha (2.17-fold), Cthb (2.22-fold), Cthc (2.78-fold), Cthd (2.35-fold) and Cthh (6.56-fold), as were the membrane scaffolding proteins Anxa1 (2.26-fold), Anxa3 (1.78-fold), and Anxa4 (2.61-fold) (Table 3). Conversely, other ECM peptides were down-regulated in Kras<sup>LA1</sup> scaffolds that were enriched in the GO terms “extracellular region” ( $p=1.09E-07$ ), “collagen type IV” ( $p=6.94E-04$ ), and “sheet-forming collagen” ( $p=6.94E-04$ ) (Fig. 3C), including collagen type IV isoforms  $\alpha 3$ ,  $\alpha 4$ , and  $\alpha 5$  (all  $> 1.6$ -fold decrease, Table 3). Thus, lung tumorigenesis was accompanied by specific changes in ECM peptide content.

Given that lung tumors in Kras<sup>LA1</sup> mice are infiltrated by a Thy-1<sup>pos</sup> population of CAFs we examined next whether CAF matrices contribute to the desmoplastic response observed in the lung scaffolds. Flow sorting was performed on the lungs of syngeneic wild-type mice and Kras<sup>LA1</sup> mice to isolate LFs and CAFs, respectively

**Figure 3.** *Strategy for global proteomic profiling of decellularized lung scaffolds.* (A) Experimental strategy for quantitative proteomic analysis of lung scaffolds. Cysteine residues in tissues were labeled with heavy and light acrylamide and quantified using liquid chromatography-mass spectrometry (LC-MS/MS). (B, C) Gene Ontology (GO) classifications (Term) significantly enriched in proteins up-regulated (B) or down-regulated (C) in Kras<sup>LA1</sup> scaffolds. Classifications listed in rank order based on p-values (modified Fisher exact test).

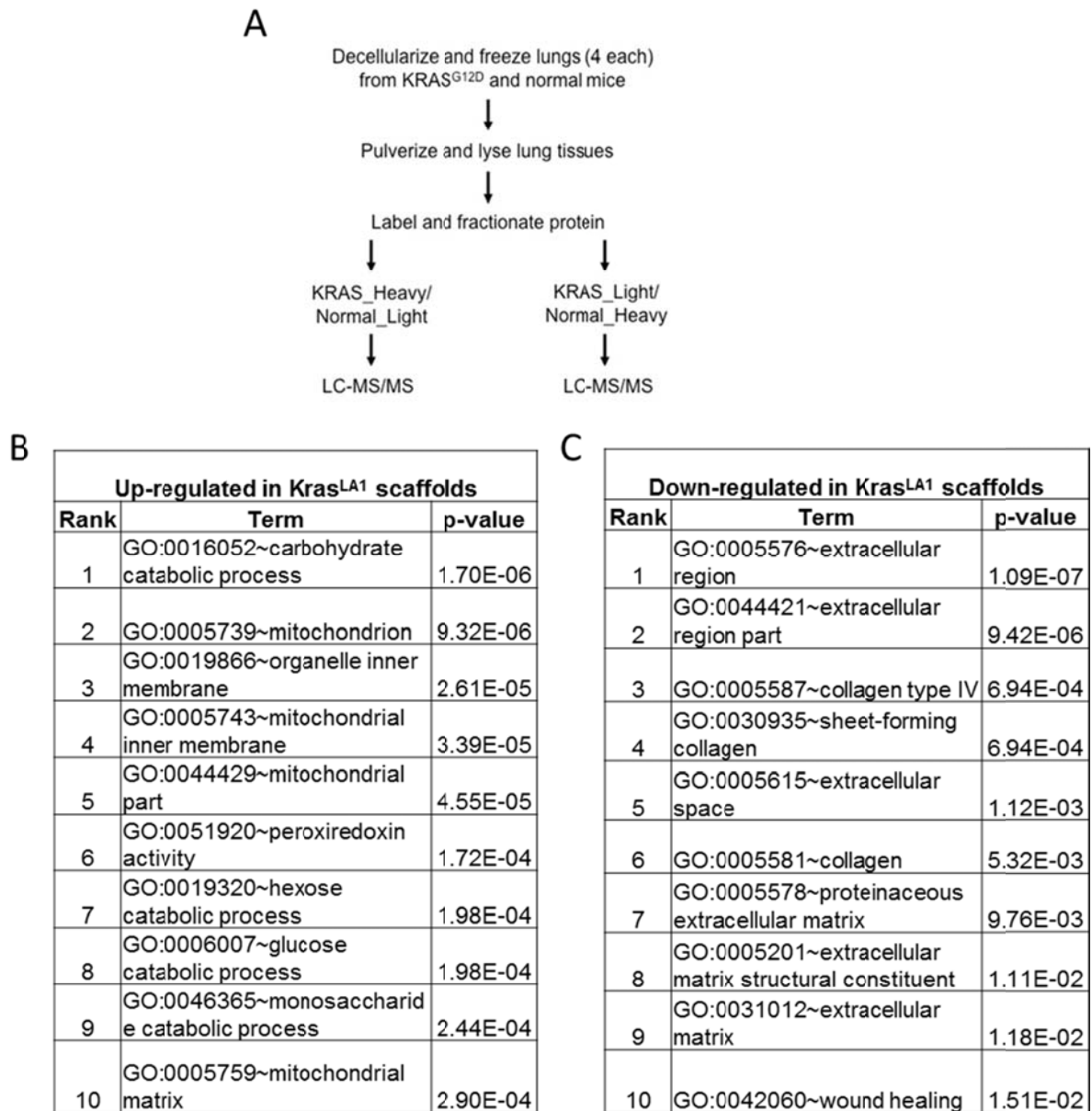


**Figure 3**

**Table 2.** *ECM-related peptides up- and down-regulated in Kras<sup>LA1</sup> scaffold profiling analysis.* LC-MS/MS analysis of Kras<sup>WT</sup> and Kras<sup>LA1</sup> scaffolds. Peptides listed are limited to those with consistent changes (> 1.5-fold up-regulation and < -1.5-fold down-regulation, p-values < 0.05, t-test) by reciprocal labeling. Normalized fold change values greater than one indicate positive up-regulation (fold regulation = fold change). Normalized fold change values less than one indicate down-regulation (fold regulation = -1/fold change).

**Table 2.** LC-MS/MS analysis of K-ras<sup>WT</sup> and K-ras<sup>LA1</sup> scaffolds (ECM-related peptides).

Gene	Fold regulation (Kras <sup>LA1</sup> / Kras <sup>WT</sup> )	p-value
<i>&gt; 1.5 fold up-regulation, p &lt; 0.05</i>		
Col1a1	2.03	9.36E-07
Fn1	1.56	4.81E-11
Bgn	1.91	1.42E-14
Tnxb	2.36	8.66E-09
Lamb1	1.50	2.68E-03
Sparc	2.11	5.62E-05
Actr3	1.75	2.16E-04
Myh14	1.78	1.06E-01
Myl6	3.26	4.44E-11
Capzb	1.65	1.42E-01
Des	2.31	6.14E-04
Dstn	2.54	7.77E-18
Tagln2	1.53	5.99E-06
Ctsa	2.17	3.81E-03
Ctsb	2.22	1.07E-03
Ctsc	2.78	1.89E-05
Ctsd	2.35	1.74E-17
Ctsh	6.56	4.62E-07
Anxa1	2.26	7.71E-07
Anxa3	1.78	2.65E-03
Anxa4	2.61	9.42E-290
<i>&lt; -1.5 fold down-regulation, p &lt; 0.05</i>		
Col4a3	-1.61	3.85E-05
Col4a4	-1.67	1.92E-07
Col4a5	-1.80	9.37E-08
Crtap	-1.71	1.20E-03
Fgb	-1.54	2.02E-22
Fgg	-1.51	1.42E-12
Pcolce2	-1.62	3.28E-06



**Table 3.** *Functional classifications of ECM-related peptides up- and down-regulated in  $Kras^{LA1}$  scaffold profiling analysis.* Cellular function-based grouping of peptides identified in Table 2) which met cut-off threshold of > 1.5 fold up-regulation or < -1.5 down-regulation with a  $p < 0.05$ , (t-test).

**Table 3.** Functional classifications of peptides identified in LC-MS/MS analysis of K-ras<sup>WT</sup> and K-ras<sup>LA1</sup> scaffolds.

Up-regulated tumor scaffold peptides ( > 1.5 fold regulation, p < 0.05)				
ECM	Basement Membrane	Actin Cytoskeleton	Cysteine Protease	Membrane Scaffold
Col1a1	Lamb1	Actr3	Ctsa	Anxa1
Fn1	Sparc	Myh14	Ctsb	Anxa3
Bgn		Myl6	Ctsc	Anxa4
Tnxb		Capzb	Ctsd	
		Des	Ctsh	
		Dstn		
		Tagln2		

Down-regulated tumor scaffold peptides ( < -1.5 fold regulation, p < 0.05)	
ECM	Basement Membrane
Pcolce2	Col4a3
Crtap	Col4a4
Fgb	Col4a5
Fgg	

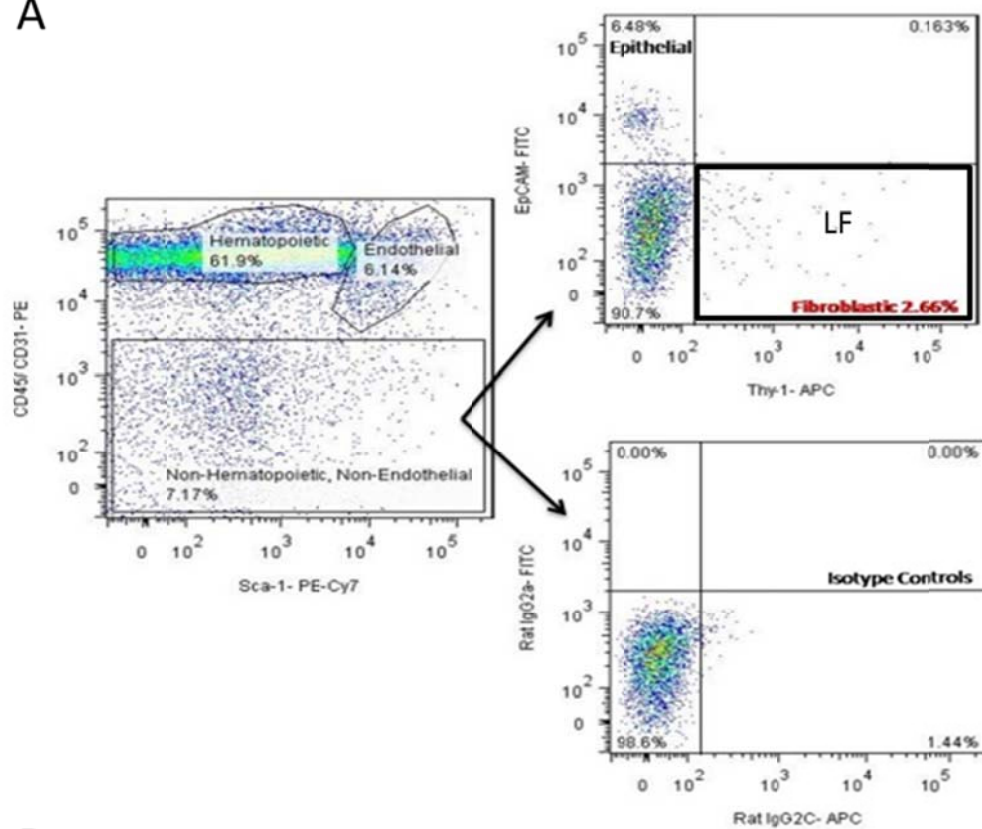
(Fig. 4 illustrates schema for cell isolation and relative abundance of sorted cells). We performed comparative mRNA expression profiling studies on CAFs and LFs by using a quantitative reverse transcriptase PCR array that includes 84 ECM-related genes. The only gene up-regulated more than 4-fold in CAFs was Col1a1 (15-fold) (Fig. 5A), which was confirmed by immunostaining of LFs and CAFs with anti-collagen type I antibodies (Fig. 6). Twelve matrix metalloproteinase (MMP) family members were down-regulated in CAFs, including MMP-1, MMP-8, and MMP-13 (Fig. 5B), which have fibrillar collagenolytic activity (31). These findings support a role for CAFs in intra-tumoral desmoplasia in Kras<sup>LA1</sup> mice.

We posited that differences in matrix content play a critical role in tumor cell adherence and invasion and tested this hypothesis by examining first the adherence of non-metastatic (393P) and highly metastatic (344SQ) KP cell lines (22) to collagen type I and other ECM molecules. Metastatic 344SQ cells were significantly more adherent to collagen type I than non-metastatic 393P cells were, and neither cell line adhered to collagen IV, laminin, or fibronectin at a higher affinity than they did to BSA control (Fig. 5C). Next, we co-cultured LFs or CAFs with a KP cell line (344SQ) that forms polarized spheres in 3-D Matrigel cultures (Fig. 7A). After polarized sphere formation, the structures were overlaid with LFs or CAFs, which revealed that the spheres acquired invasive properties in co-culture with CAFs but not LFs (Fig. 7B). To determine whether CAF matrices are sufficient to mediate tumor cell invasion, purified matrices isolated from CAF mono-cultures were overlaid on polarized spheres. The spheres that were in direct contact with the CAF matrix acquired invasive phenotypes, whereas spheres that were not in contact with

**Figure 4.** *Prospective isolation strategy for LF and CAF stromal cell compartments.*

Flow cytometric isolation of  $CD45^{Neg}CD31^{Neg}Ep-CAM^{Neg}Thy-1^{Pos}$  fibroblasts from digested lung tissues of wildtype mice (A) and  $Kras^{LA1}$  mice (B). Fluorochrome labeled antibody intensity is illustrated on logarithmic scale. Cell populations are labeled based on cell surface phenotype identification (hematopoietic,  $CD45^{Pos}$ ; endothelial,  $CD31^{Pos}Sca-1^{Pos}$ ; epithelial,  $Ep-CAM^{Pos}$ ; and fibroblastic,  $Thy-1^{Pos}$  [red, boxed]). Arrows indicate subgating of non-hematopoietic and non-endothelial cells only. Relative frequencies of cell populations are indicated (left plots, % of total viable cells; right plots, % of non-hematopoietic, non-endothelial subgates).

A



B

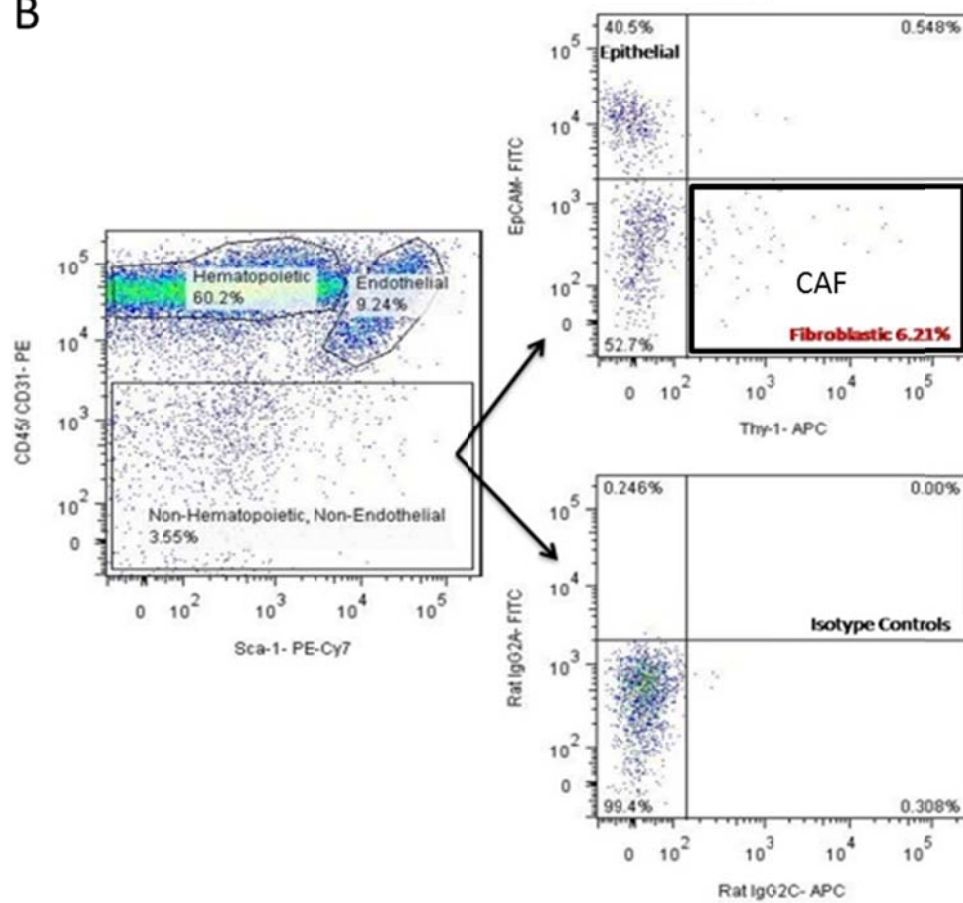


Figure 4

**Figure 5.** *CAFs secrete abundant collagen type I and down-regulate collagenolytic MMP family members.* (A) Quantitative RT-PCR analysis of RNA samples from LFs and CAFs using an ECM-specific microarray. Logarithmic scale scatter plot displaying all genes on array as  $2^{\Delta\text{Ct}}$  values for CAFs (y-axis) and LFs (x-axis). Central line indicates unchanged gene expression. Cut-off set at 4-fold up- or down-regulation (outer lines). Genes up-regulated > 4-fold (red); down-regulated > 4-fold (green); or up-regulated < 4-fold or –down-regulated < 4-fold (grey). All genes were normalized to GAPDH and  $\beta$ -actin endogenous house-keeping genes.  $C_T$  values >35 were considered non-detectable and are not illustrated. (B) Bar graph illustration of down-regulated genes in (A). MMPs with and without fibrillar collagenolytic activity are illustrated. Results expressed as fold-change in CAFs relative to LFs, which was set at 0. (C) Adherent cells were stained with crystal violet and quantified colorimetrically 1 h after seeding on plastic or coated with indicated ECM molecules or bovine serum albumin (BSA) as a control. Results expressed as mean values ( $\pm$  S.D.) of triplicate wells. P-values are indicated (t-test).

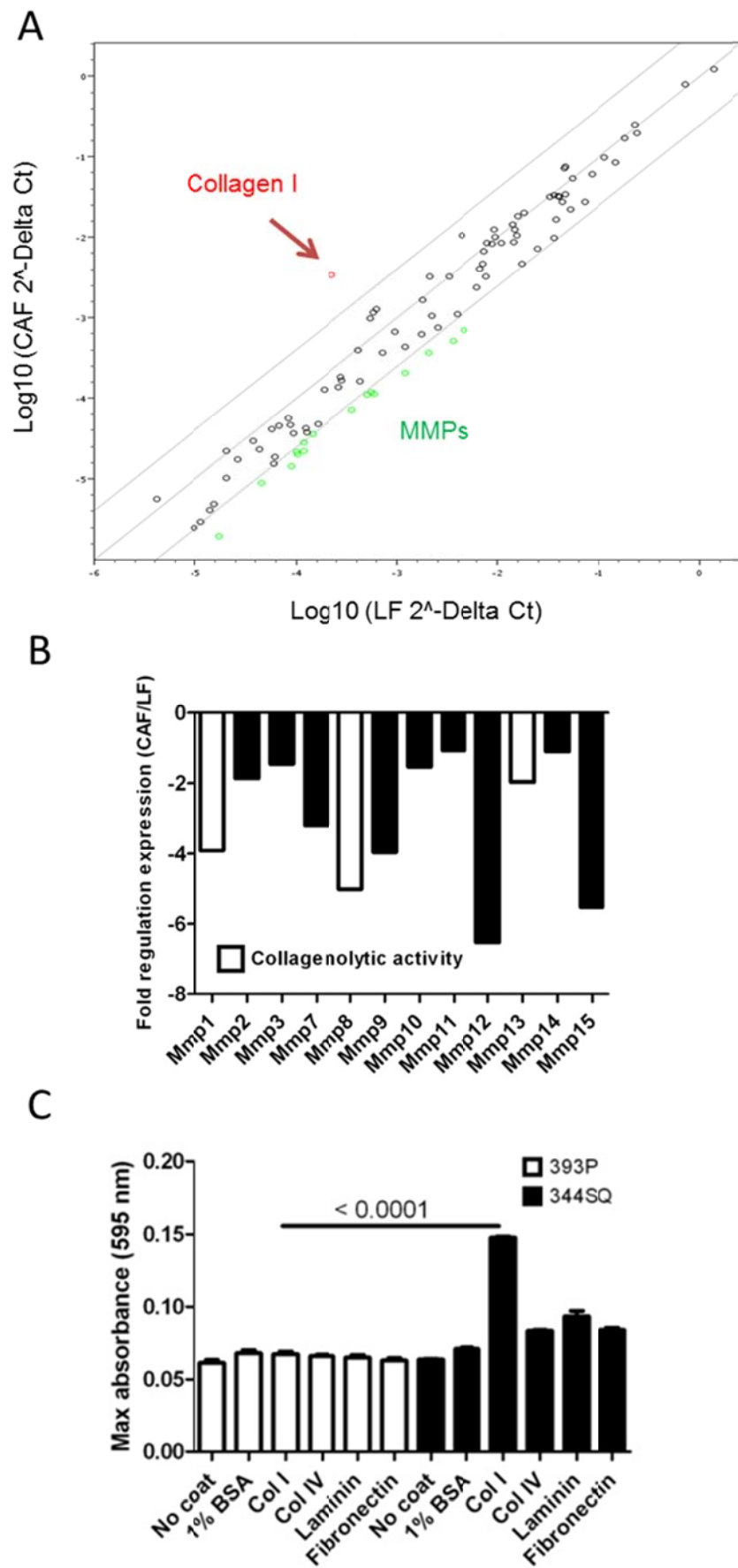
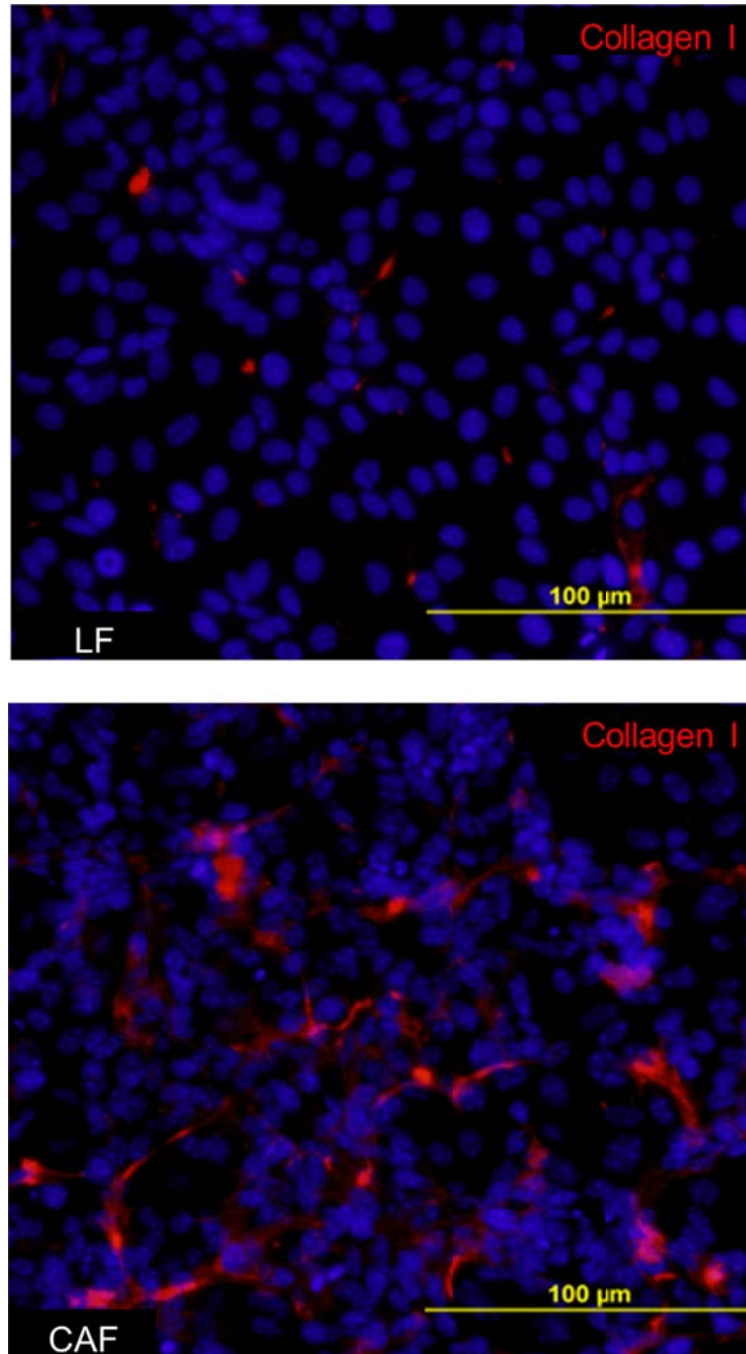


Figure 5

**Figure 6.** *CAF fibrillar collagen I secretion in vitro.* Images of LFs (top panel) and CAFs (bottom panel) grown in monolayer culture that were immunofluorescently stained using an anti-collagen type I antibody (red). DAPI (blue).





**Figure 6**

**Figure 7.** *CAFs induce tumor cell invasion through contact-dependent matrix secretion.* (A) Light microscopic image of metastatic 344SQ tumor cells seeded into Matrigel and allowed to form polarized epithelial spheres. (B) Spheres were overlaid with LFs (left panel) or CAFs (right panel). Spherical morphology was disrupted by CAFs but not LFs. (C) Polarized spheres were overlaid with matrices extracted from CAFs. Representative images of spheres that do not (left panel) or do (right panel) have direct contact with matrices. Arrow (right panel) indicates invasive outgrowth. Size bars are indicated.

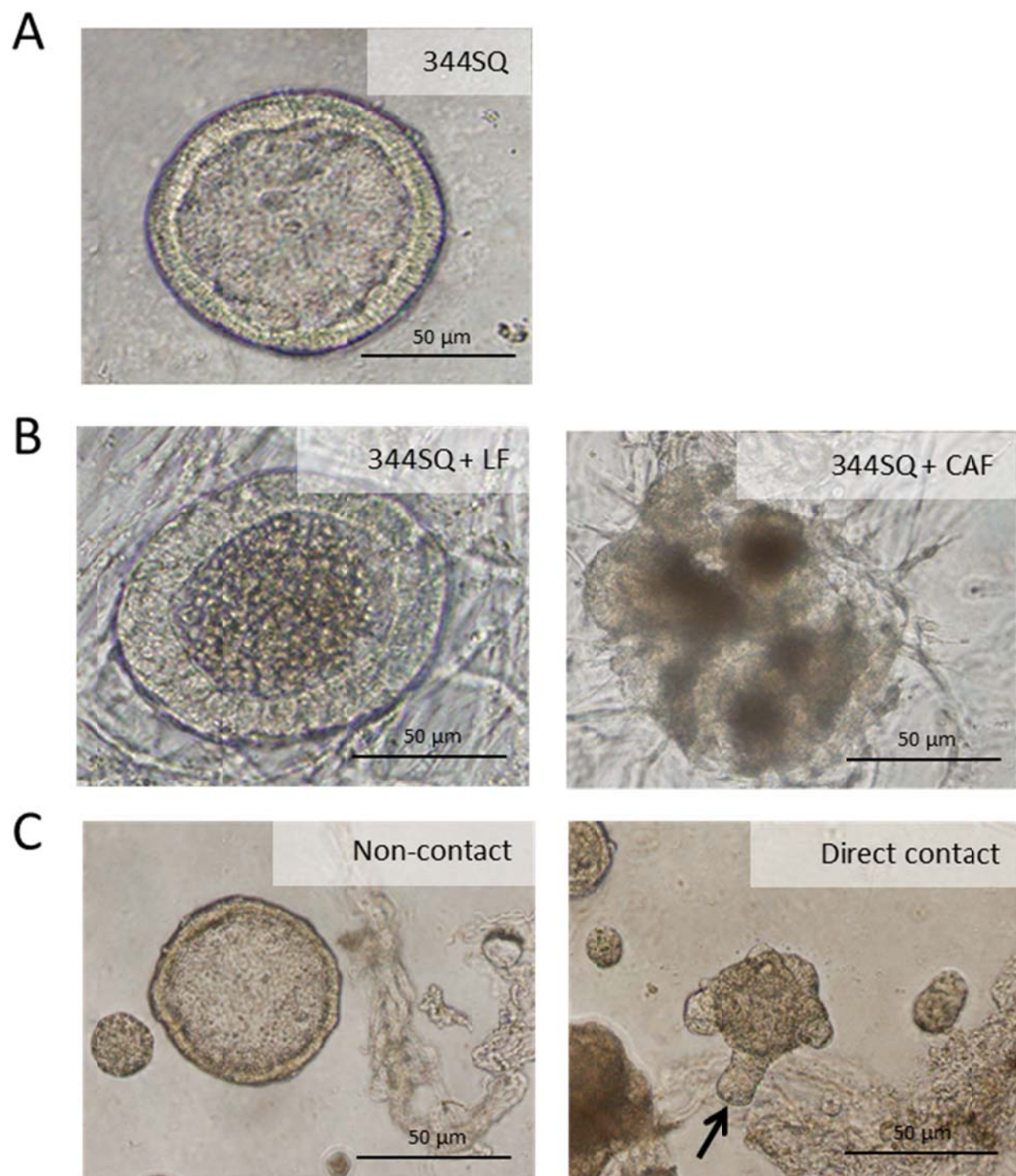


**Figure 7**

matrix did not change (Fig. 7C). These findings support the conclusion that CAF matrices promote tumor cell adherence and invasion.

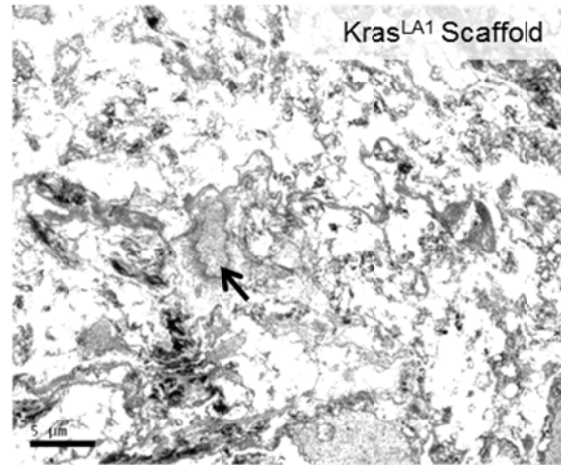
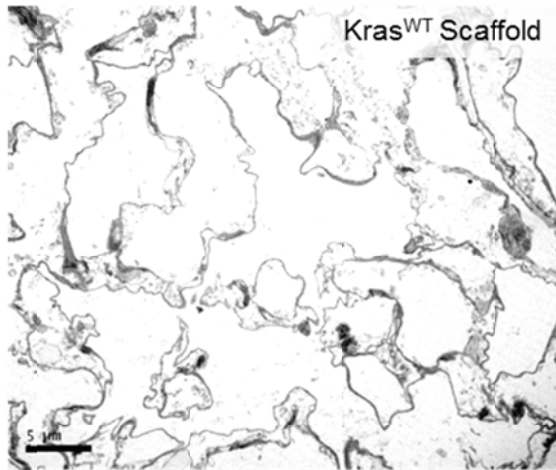
### **Aberrant organization of basement membranes in tumor ECM**

To examine ECM ultrastructural features, transmission electron microscopic analysis was performed on wild-type and Kras<sup>LA1</sup> scaffolds. Features unique to Kras<sup>LA1</sup> scaffolds included an abundance of amorphous material dispersed throughout the matrix (Fig. 8A) and basement membranes that exhibited a loss of lamina densa electron-dense bodies (Fig. 8B) and an increase in thickness (Fig. 8C) indicative of a loss of the normal, compact organization. Immunofluorescent staining of lung tissues from Kras<sup>LA1</sup> mice demonstrated that the basement membrane component collagen IV was less abundant in tumor tissues than it was in normal adjacent lung (Fig. 8D). One possible explanation for these findings is reduced secretion of basement membrane proteins by CAFs, which we examined by performing LC-MS/MS analysis on matrices purified from CAFs and LFs. A total of 1,030 peptides were differentially expressed (G value >1.65, fold-change >1.5, Table 4). Gene Ontology classifications for the top 100 up-regulated CAF peptides demonstrated enrichment in “actin polymerization” (p=1.32E-03), “cytoskeletal protein binding” (p=1.95E-05) and “cell cortex” (p=3.92E-04) (Fig. 9A), whereas down-regulated peptides were enriched in “extracellular matrix” (p=7.39E-07) and “calcium ion binding” (p=7.31E-05) (Fig. 9B). With respect to specific peptides that were differentially expressed, CAF-derived matrices had increased abundance of proteins that regulate cell motility, including spectrin protein Spna2 (2.42-fold) and

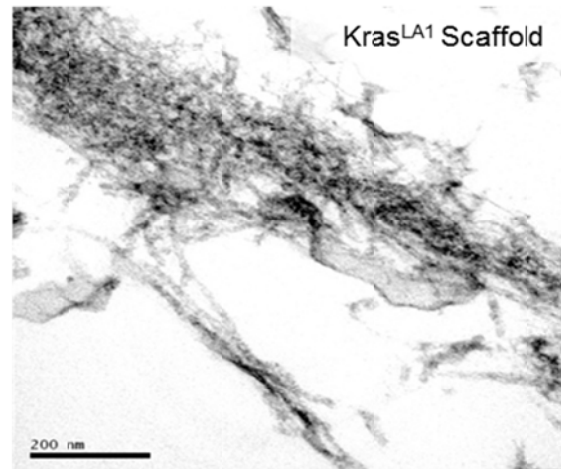
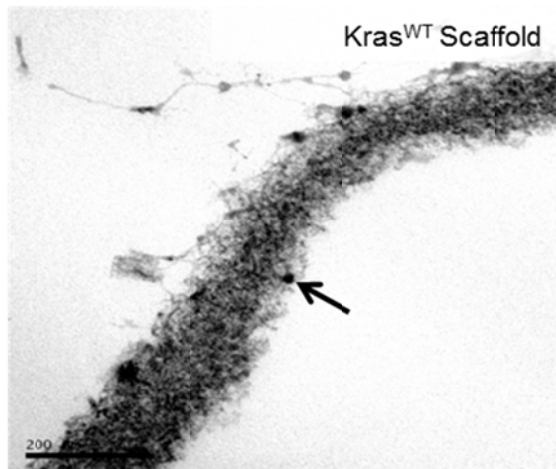
**Figure 8.** *Loss of basement membrane organization within tumor ECM.* (A) Ultrastructural features of Kras<sup>WT</sup> scaffolds (left panel) and Kras<sup>LA1</sup> scaffolds (right panel) demonstrating abundant collagen I fibers and amorphous material (arrow, right panel) in Kras<sup>LA1</sup> scaffolds. (B) Basement membranes in Kras<sup>WT</sup> scaffolds (left panel) and Kras<sup>LA1</sup> scaffolds (right panel). Collagen fibers in Kras<sup>WT</sup> scaffolds are compressed and have lamina densa-associated electron-dense bodies (arrow). Basement membranes in Kras<sup>LA1</sup> scaffolds are less organized (right versus left panels) and lack electron dense bodies. Size bars are indicated. (C) Diameters of basement membranes in Kras<sup>WT</sup> and Kras<sup>LA1</sup> scaffolds. Diameters represent mean values  $\pm$  S.D. of replicates (n=3 per genotype). (D) Reduced collagen type IV expression in tumors. Representative immunofluorescent images of lung tumor and adjacent normal lung tissues in Kras<sup>LA1</sup> mice subjected to immunofluorescent staining with anti-collagen type IV antibodies (green) and DAPI (blue). N, normal lung; T, tumor.



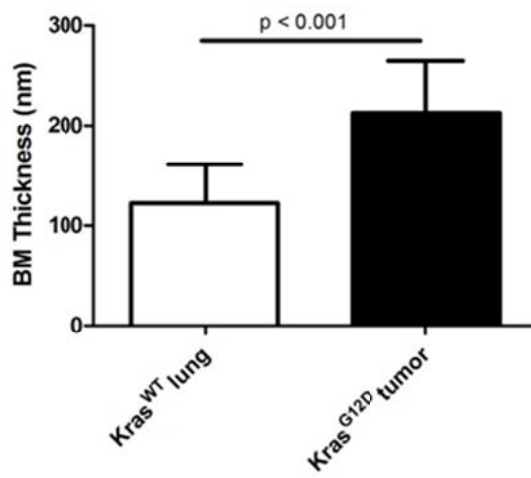
A



B



C



D

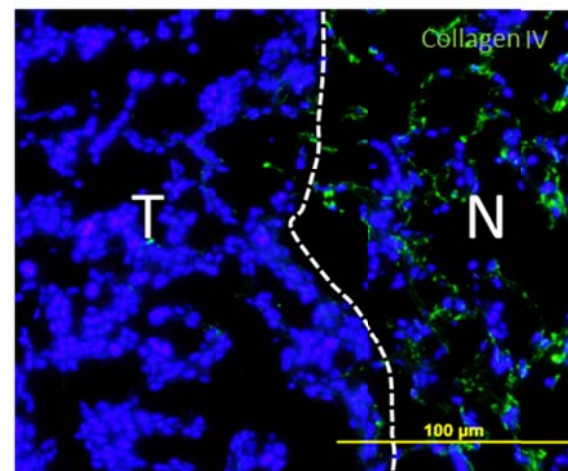


Figure 8

**Figure 9.** *Global proteomic profiling of enriched fibroblast matrices.* Gene Ontology (GO) classifications (Term) of top 100 up-regulated (A) or down-regulated (B) peptides based on LC-MS/MS analysis of matrices extracted from LFs and CAFs in mono-culture. Classifications listed in rank order based on p-values (modified Fisher exact test).

A

Rank	Term	p-value
<b><i>Up-regulated in CAF matrices, top 100 peptides</i></b>		
1	GO:0008064~regulation of actin polymerization or depolymerization	1.32E-03
2	GO:0043228~non-membrane-bounded organelle	4.32E-07
3	GO:0043232~intracellular non-membrane-bounded organelle	4.32E-07
4	GO:0003779~actin binding	6.90E-06
5	GO:0008092~cytoskeletal protein binding	1.95E-05
6	GO:0005938~cell cortex	3.92E-04
7	GO:0015629~actin cytoskeleton	5.17E-04
8	GO:0005730~nucleolus	8.22E-04
9	GO:0030832~regulation of actin filament length	1.40E-03
10	GO:0032956~regulation of actin cytoskeleton organization	2.23E-03

B

Rank	Term	p-value
<b><i>Down-regulated in CAF matrices, top 100 peptides</i></b>		
1	GO:0031012~extracellular matrix	7.39E-07
2	GO:0005578~proteinaceous extracellular matrix	3.53E-06
3	GO:0044421~extracellular region part	3.53E-05
4	GO:0031967~organelle envelope	4.54E-05
5	GO:0031975~envelope	4.72E-05
6	GO:0005509~calcium ion binding	7.31E-05
7	GO:0005739~mitochondrion	8.93E-05
8	GO:0044420~extracellular matrix part	3.37E-04
9	GO:0044432~endoplasmic reticulum part	7.87E-04
10	GO:0005788~endoplasmic reticulum lumen	1.26E-03

Figure 9



**Table 4.** *ECM-related peptides up- and down-regulated in CAF matrix profiling analysis.* LC-MS/MS analysis of normal and cancer-associated fibroblast matrices. Peptides listed are limited to mouse origin only (removing bovine peptides derived from FBS) with changes ( $> 1.5$  fold up-regulation and  $< -1.5$  down regulation, G-values  $>1.65$ , g-test). Normalized fold change values greater than one indicate positive up-regulation (fold regulation = fold change). Normalized fold change values less than one indicate down-regulation (fold regulation =  $-1/\text{fold change}$ ). \* indicates peptides differentially expressed in Kras<sup>LA1</sup> scaffolds (Table 2).

**Table 4.** LC-MS/MS analysis of LF and CAF matrices (ECM-related peptides).

Gene	Fold regulation (CAF / LF)	g-value
<i>&gt; 1.5 fold up-regulation g &gt; 1.65</i>		
Col1a2*	5.10	3.77
Col5a1	4.08	2.50
Col5a3	4.08	2.50
Tnxb*	4.08	2.50
Spna2	2.42	8.02
Ankar	4.08	2.50
Cdh23	7.15	6.54
Dstn*	2.16	33.54
Fblim1	1.58	2.11
Arhgef12	4.08	2.50
Arhgap17	3.93	6.07
Arhgap18	3.01	4.48
Ktn1	9.21	9.50
Ctse	2.41	2.54
Ctsh*	10.23	11.03
Ctsl	1.66	12.20
Anxa4*	2.08	17.85
Anxa11	5.10	3.77
<i>&lt; -1.5 fold down-regulation, g &gt; 1.65</i>		
Col6a1	-21.80	29.25
Col6a2	-17.00	21.54
Col6a3	-21.80	29.25
Col9a2	-5.00	3.64
Col18a1	-2.01	1.77
Emilin1	-4.20	2.65
Fgg*	-5.80	4.69
Arhgef1	-4.20	2.65
Arhgdia	-2.18	4.56
Col4a2*	-1.99	2.56
Hspg2	-3.31	23.34
Nid1	-13.00	15.25
Lama3	-3.40	1.73
Lama5	-10.60	11.59
Lamb1	-1.82	3.08
Lamb2	-2.25	3.79
Lamc1	-11.86	41.21
Lamc2	-3.40	1.73
Lbr	-8.20	8.04

destrin (2.16-fold), membrane scaffolding proteins (Anxa4 and Anxa11, 2.08- and 5.10-fold, respectively), and a protease (cathepsin H, 10.23-fold) reported to be highly expressed in tumors from Kras<sup>LA1</sup> mice (32) (Table 5). Conversely, several basement membrane components were down-regulated, including collagen IV (1.99-fold), which was also down-regulated in Kras<sup>LA1</sup> scaffolds (Table 6), and basement membrane-associated proteoglycans HSPG2 (3.31-fold) and nidogen-1 (13.00-fold) and laminin subunits Lama3 (3.40-fold), Lama5 (10.60-fold), Lamb1 (1.82-fold), Lamb2 (2.25-fold), Lamc1 (11.86-fold), and Lamc2 (3.40-fold) (Table 5). Thus, the CAF secretome contained widespread changes in ECM content (schematically illustrated in Fig. 10).

### **Multi-functional role of fibulin-2 during malignant progression**

Given the above ultrastructural evidence that tumor ECM is highly disorganized, we posited that matrix-stabilizing factors regulate malignant progression (schematically illustrated in Fig. 11). Abundantly secreted by metastatic KP cells, fibulin-2 is thought to stabilize the assembly of a variety of macromolecular structures, including tropo-elastin fibers, microfibrils, and matrix-proteoglycan complexes and is required for cardiac tissue remodeling during myocardial infarction, a hypoxic condition analogous to that observed in epithelial tumor ECM (33). Western blot analysis of KP cell lines revealed that fibulin-2 was more abundantly expressed in metastasis-prone (mesenchymal) KP cells than it was in non-metastatic (epithelial) KP cells (Fig. 12A). Consistent with known splice isoforms of fibulin-2, there were 2 bands of approximately 190 kD and 150 kD in

**Table 5.** *Functional classifications of ECM-related peptides up- and down-regulated in CAF matrix profiling analysis.* Cellular function-based grouping of peptides identified in Table 4) which met cut-off threshold of > 1.5 fold up-regulation or < -1.5 down-regulation with a g-value >1.65, (g-test). \* indicates peptides differentially expressed in Kras<sup>LA1</sup> scaffolds (Table 2).

**Table 5.** Functional classifications of peptides identified in LC-MS/MS analysis of LF and CAF matrices.

<b>Up-regulated CAF matrix peptides ( &gt; 1.5 fold regulation, g &gt; 1.65)</b>			
ECM	Actin Cytoskeleton	Cysteine Protease	Membrane Scaffold
Col1a2*	Spna2	Ctse	Anxa4*
Col5a1	Ankar	Ctsh*	Anxa11
Col5a3	Cdh23	Ctsl	
Tnxb*	Dstn*		
	Fblim1		
	Ktn1		
	Arhgef12		
	Arhgap17		
	Arhgap18		

<b>Down-regulated CAF matrix peptides ( &lt; -1.5 fold regulation, g &gt; 1.65)</b>		
ECM	Actin Cytoskeleton	Basement Membrane
Col6a1	Arhgdia	Col4a2*
Col6a2	Arhgef1	Hspg2
Col6a3		Nid1
Col9a2		Vcan
Col18a1		Lama3
Emilin1		Lama5
Fgg*		Lamb1
		Lamb2
		Lamc1
		Lamc2
		Lbr

**Table 6.** *Proteomic profiling comparison of in vivo scaffolds vs in vitro matrices analysis.* Comparison of peptides and corresponding functional classifications up (+) and down (-) regulated within Kras<sup>LA1</sup> tumor scaffolds and CAF matrices.

**Table 6.** Proteomic profiling comparison of *in vivo* scaffolds vs. *in vitro* matrices analysis.

Cellular Function	Proteins	Tumor / Normal Scaffolds	CAF / LF Matrices
ECM / stiffness	Collagen I	+	+
Actin cytoskeleton	Destrin	+	+
Membrane scaffold	Annexins	+	+
Basement membrane	Collagen IV	-	-
Cysteine protease	Cathepsins	+	+

**Figure 10.** *Schematic illustration of CAF dependent effects on tumor-associated ECM.* CAF-derived collagen I is stabilized through down-regulation of collagenolytic MMPs resulting in increased tumor desmoplastic scarring and CAF motility through cytoskeletal elements. CAFs down-regulate basement membrane components and up-regulate cathepsin h for increased tumor cell invasion. Collectively, CAFs provide an intricate balance of ECM deposition, stabilization, down-regulation, and degradation to provide an optimal microenvironment for tumor progression.



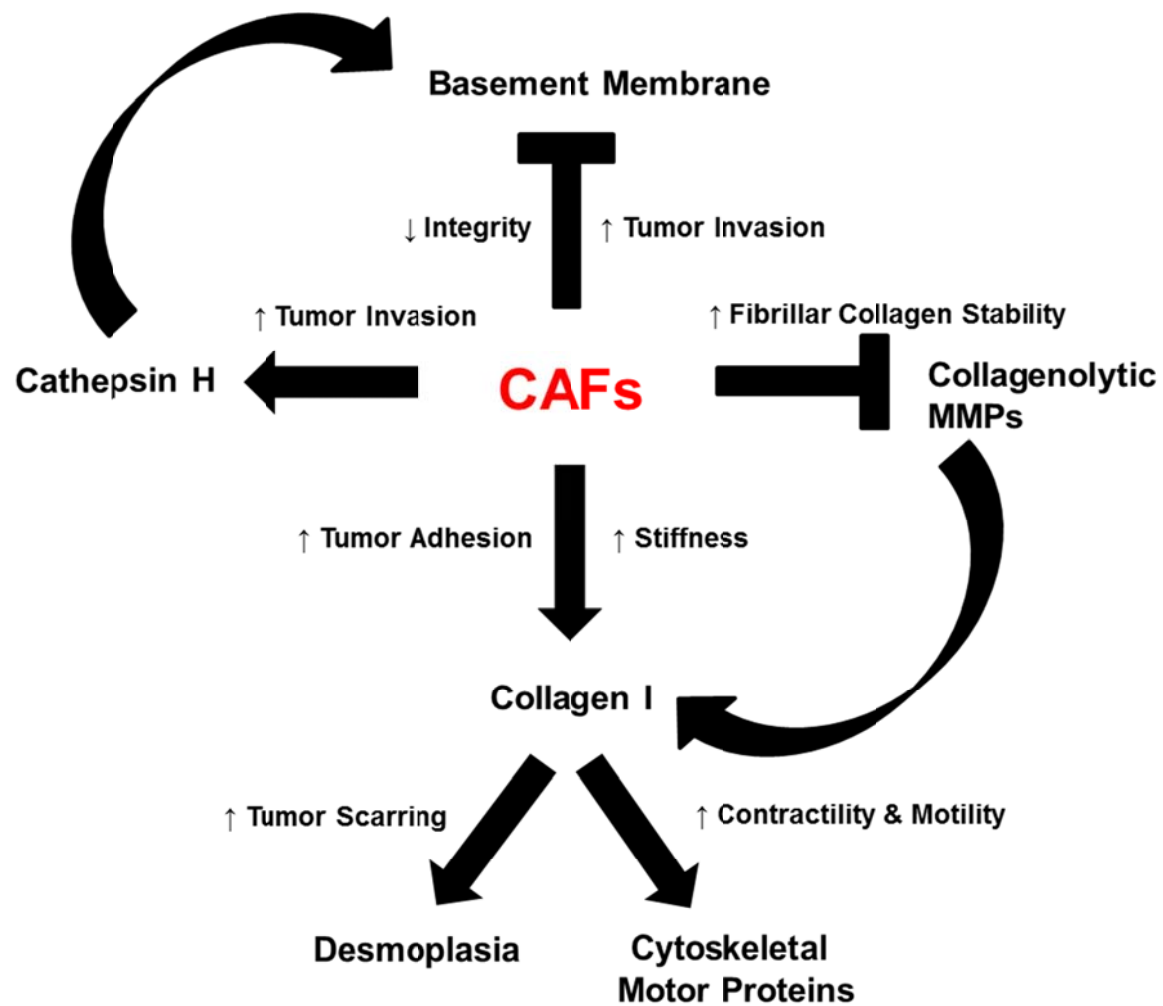


Figure 10

**Figure 11.** *Schematic illustration of proposed feed-forward model of tumor cell-derived ECM stabilizing factors which regulate matrix stabilization.* Unknown ECM stabilizing factors interact with a mature, collagen-rich matrix derived primarily from cancer-associated fibroblasts, which stimulates tumor cells to secrete additional ECM molecules thereby engendering matrix stabilization.

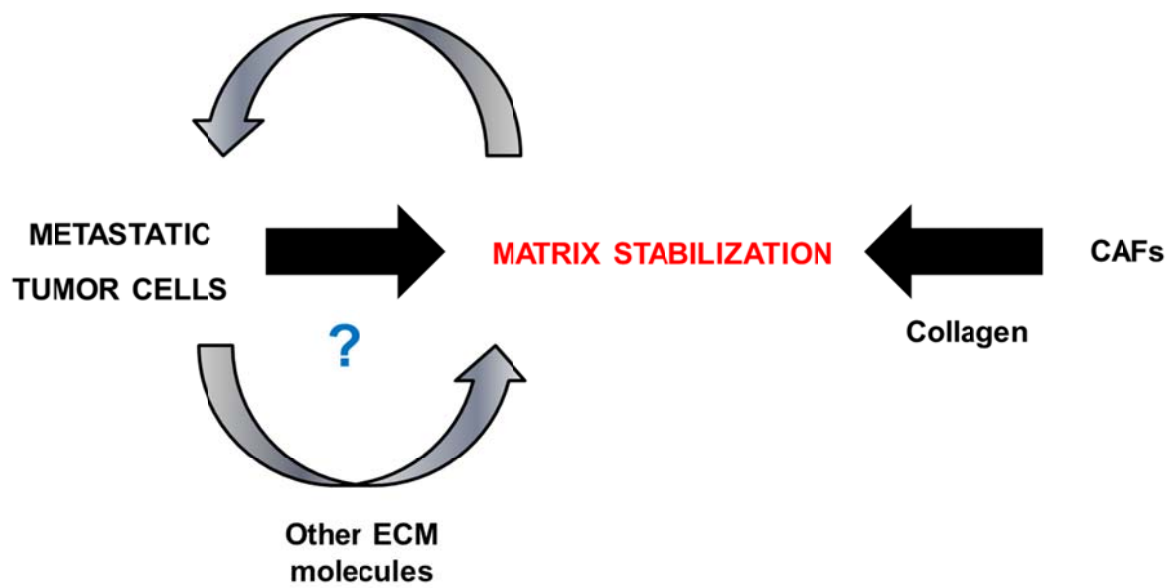
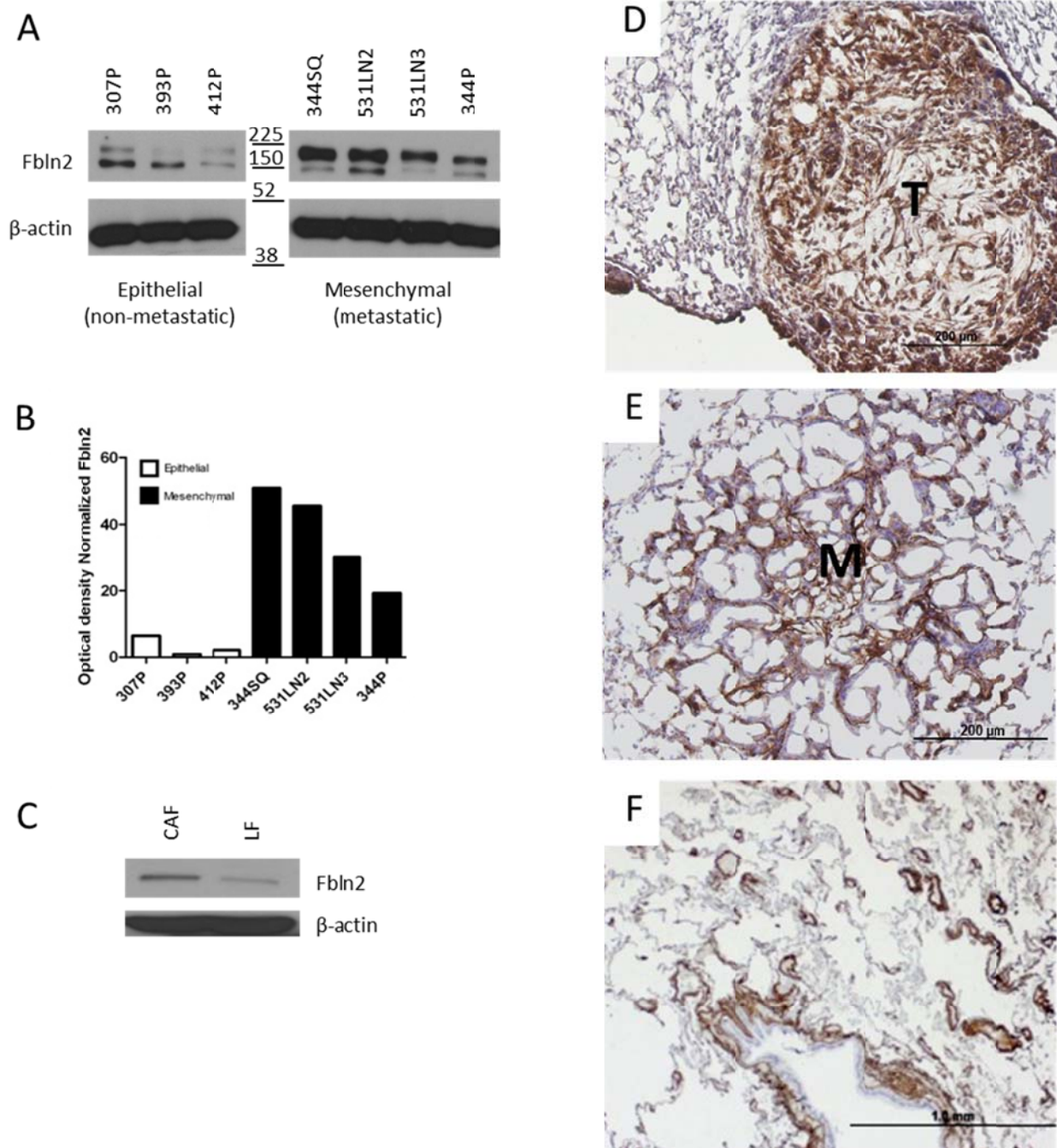


Figure 11

**Figure 12.** *Fibulin-2 production in murine lung adenocarcinomas and normal tissue specimens.* (A) Western blot analysis of fibulin-2 expression in KP cell lines. Two fibulin-2 species identified that differ on the basis of molecular weight (190 kD and 150 kD).  $\beta$ -actin included as loading control. (B) Densitometric analysis of western blot in (A). Larger molecular weight band normalized on the basis of  $\beta$ -actin. (C) Western blot analysis of fibulin-2 in CAFs and LFs. A single 190 kD band was detected.  $\beta$ -actin included as loading control. (D-F) Anti-fibulin-2 immunohistochemical staining (brown) of a lung adenocarcinoma from a KP mouse (D), a nascent metastasis to lung in a syngeneic wild-type mouse injected subcutaneously with 344SQ cells (E), and normal human lung adjacent to tumor (F).



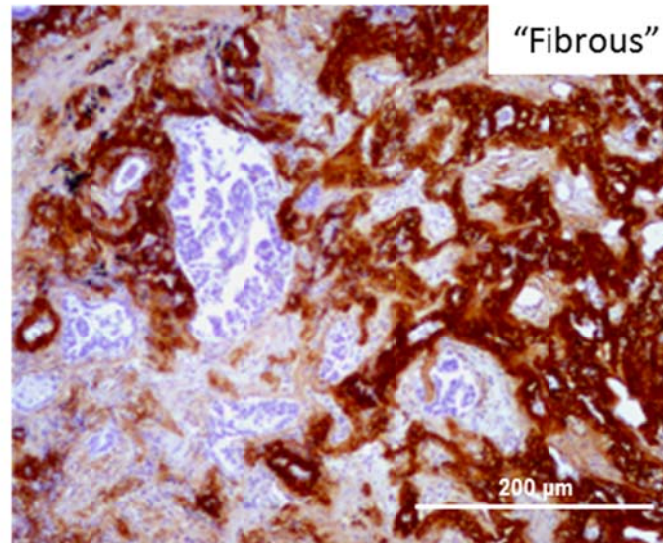
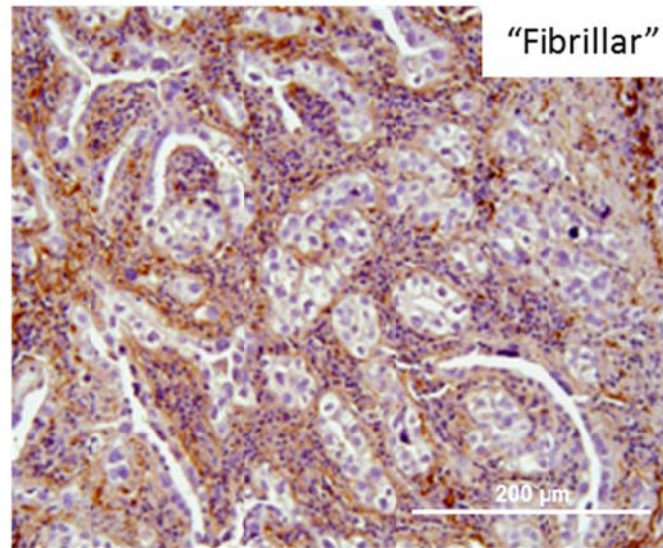
**Figure 12**

size, and the relative abundance of the larger band correlated with metastatic propensity (Fig. 12B). Beyond its increase in metastasis-prone tumor cells, fibulin-2 was more abundantly expressed in CAFs than it was in LFs (Fig. 12C). Next, we performed immunohistochemical studies on human and murine lung tissues to examine fibulin-2 abundance and intra-tumoral localization. Fibulin-2 was detected in primary lung tumors in KP mice (Fig. 12D) and in lung metastases from mice injected subcutaneously with 344SQ cells (Fig. 12E). In human lung tissues, fibulin-2 was detected in elastic tissues within bronchi and vascular structures adjacent to tumor (Fig. 12F), in a “fibrillar” pattern between tumor cells and surrounding tumor acini, and in a “fibrotic” pattern within intra-tumoral fibrotic bands (Fig. 13A). On the basis of Kaplan-Meier analysis of 46 resected primary human lung adenocarcinomas, time-to-disease recurrence correlated negatively with “fibrotic” fibulin-2 staining (Fig. 13B).

To test our hypothesis that matrix-stabilizing factors regulate malignant progression, we inhibited fibulin-2 in metastasis-prone KP cells. Fibulin-2-deficient KP cells were generated by stable transfection of one of six different shRNAs that target distinct *Fbln2* mRNA sequences. Two 344SQ transfectants (shFbln2 #1 and #2) that achieved at least 50% knockdown relative to scrambled controls (shSCR) (Fig. 14A-C) were injected subcutaneously or intra-thoracically into syngeneic wild-type mice to generate subcutaneous or intra-thoracic orthotopic tumors, respectively. Relative to control shRNA-transfected tumors, fibulin-2-deficient tumors were significantly smaller and generated fewer metastases regardless of injection site (Fig. 15A-B). Confirmatory studies on a second KP cell line that has

**Figure 13.** *Fibulin-2 is highly expressed in human lung adenocarcinomas and correlates with poor clinical outcome.* (A) Anti-fibulin-2 immunohistochemical staining (brown) of two different primary human lung adenocarcinomas representative of fibrillar (top panel) and fibrous (bottom panel) staining patterns. Size bars are indicated. (B) Surgically resected human lung adenocarcinomas (n=46) fully annotated for demographic variables, pathologic stage, smoking status, and clinical outcome were immunohistochemically stained using anti-fibulin-2 antibodies and quantitatively scored based on staining intensity and pattern. Kaplan-Meier analysis (graph) of time-to-disease recurrence based on intensity of fibrous fibulin-2 staining.

A



B

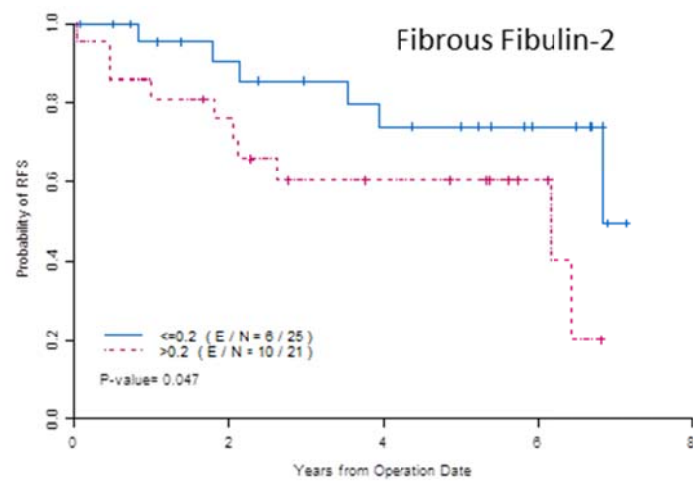
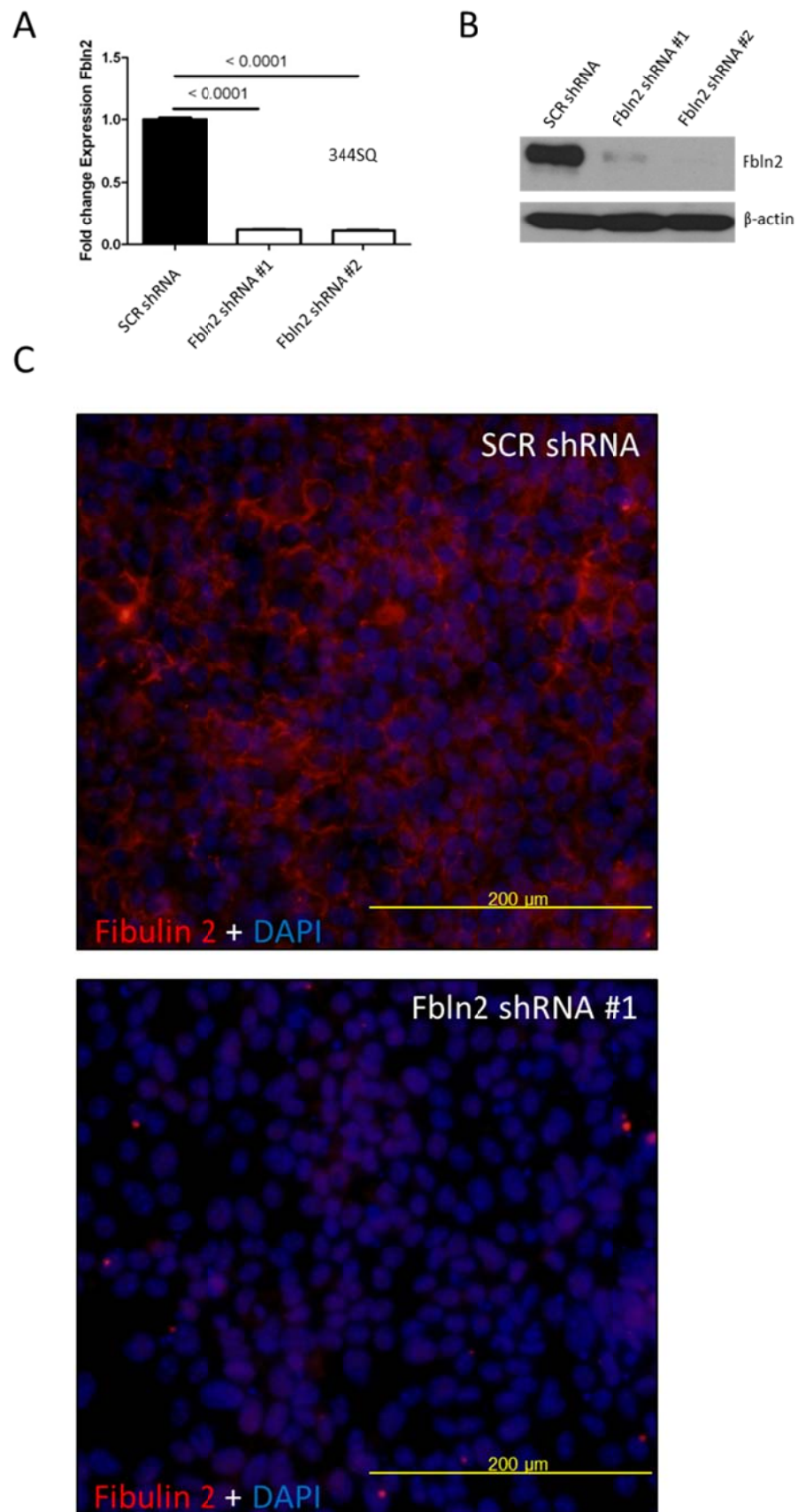


Figure 13



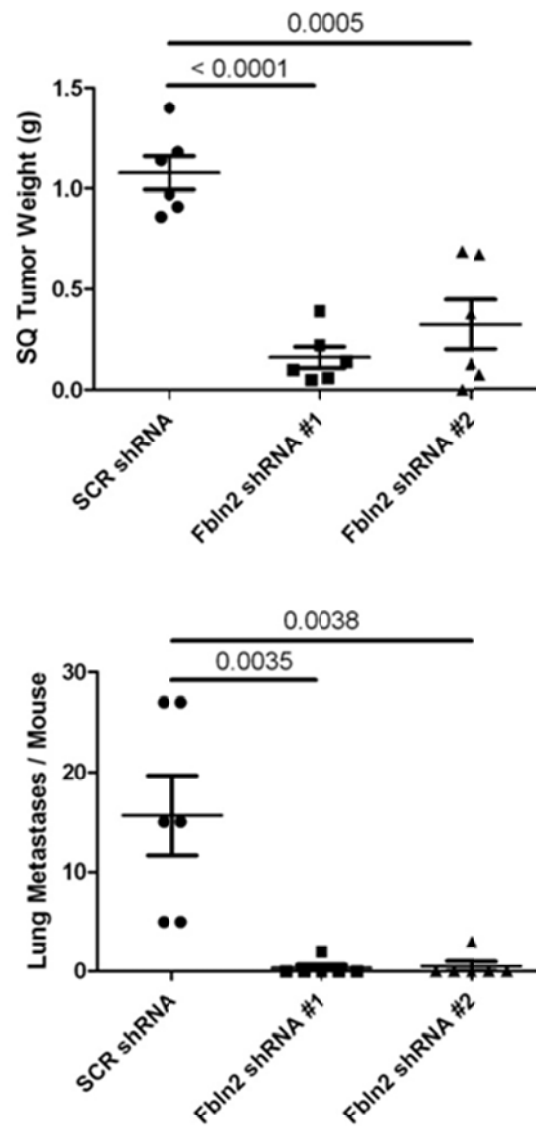
**Figure 14.** *Derivation of fibulin-2 shRNA knock down cells in a highly metastatic KP cell line.* (A) Quantitative RT-PCR assays on 344SQ cells stably transfected with scrambled control shRNA (SCR shRNA) or Fbln2 shRNA #1 or #2. Values normalized on the basis of L32 ribosomal RNA and expressed as the mean values ( $\pm$  S.D.) of quadruplicate samples. Western blotting (B) and immunofluorescence staining (C) of fibulin-2 in 344SQ cells stably transfected with control (SCR) or Fbln2 shRNA #1 or #2. Anti-fibulin-2 (red) and DAPI (blue).



**Figure 14**

**Figure 15.** *Fibulin-2 promotes the growth and metastatic properties of KP cells.* (A) Transfectants ( $10^6$ ) injected into the flank of syngeneic wild-type mice (n=10 per cohort) to generate subcutaneous tumors. Mice sacrificed after 6 weeks to weigh primary tumor (top bar graph) and count visible lung metastases (bottom bar graph). Scatter plot representation of each tissue sample (squares), mean values (long line) and standard deviations (short line). P-values are indicated (t-test). (B) Syngeneic mice (n=10 per cohort) were injected intra-thoracically with transfectants ( $2 \times 10^4$ ) to generate a single orthotopic lung tumor. Mice were sacrificed after 2 weeks to identify metastases to mediastinal lymph nodes and distant sites. Percentages of mice in each cohort with metastases to mediastinal lymph nodes (bar graph). P-values are indicated (t-test).

A



B

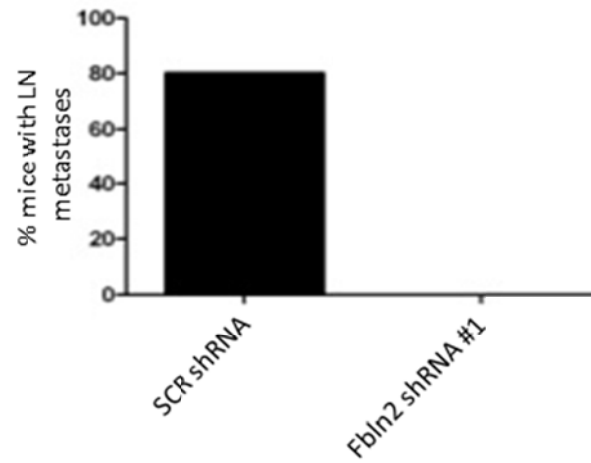


Figure 15

high fibulin-2 expression (531LN2) revealed that shRNA-mediated depletion of fibulin-2 reduced the growth and metastasis of 531LN2 cells in syngenic mice (Fig. 16A-D). Furthermore, fibulin-2-deficient 344SQ cells exhibited reduced proliferation in monolayer cultures (Fig. 17A), formed fewer colonies in soft agar (Fig. 17B and Fig. 18A), and were less invasive in Boyden chamber assays (Fig. 17C and Fig. 18B). These profound changes in tumor cell biology justified investigations into potential sequelae of fibulin-2 deficiency on tumor ECM content and structure.

### **Fibulin-2 stabilizes tumor ECM**

Fibulin-2-deficient and –replete flank tumors were stained with Picosirius Red to visualize collagen content. Quantification using Image J software revealed that fibulin-2 deficiency reduced dense fibrous stroma deposition (Fig. 19A-C), which resulted in a less compact ECM. Fibulin-2-deficient orthotopic lung tumors were significantly less stiff than control tumors (Fig. 20A), and conditioned media samples from fibulin-2-deficient cells were enriched in soluble (non-cross-linked) collagen following pepsin digestion of exposed (uncross-linked) telopeptides (Fig. 20B). The pronounced impact of fibulin-2 deficiency on collagen maturation was surprising given that fibulin-2 does not colocalize to collagen type I fibers (34) and raised the possibility that fibulin-2 deficiency changed the abundance of lysyl oxidase cross-linked enzymes. To this end fibulin-2 deficient cells had reduced LOXL-3 and -4 expression (Fig. 20C). We also explored whether fibulin-2 deficiency influenced other ECM components required for matrix organization and remodeling. Indeed, fibulin-2-deficient cells had reduced expression and secretion of many basement

**Figure 16.** *Fibulin-2 shRNA knock down in an additional metastatic KP cell line.* (A) Quantitative RT-PCR assays of 531LN2 cells stably transfected with Fbln2 shRNA #3 and #4. Values normalized on the basis of L32 ribosomal RNA and expressed as the mean values ( $\pm$  S.D.) of quadruplicate samples. (B) Western blotting of 531LN2 cells transfected with scrambled control shRNA (SCR shRNA) or Fbln2 shRNA #3 or #4.  $\beta$ -actin included as a loading control. (C, D) Transfectants ( $10^6$ ) injected into the flank of syngenic mice (n=10 per cohort) to generate subcutaneous tumors. Mice sacrificed after 6 weeks to weigh primary tumors (C) and count lung metastases (D). Scatter plot representation of each tissue sample (dots, squares, triangles), mean values (long line), and standard deviations (short line). P-values are indicated (t-test).

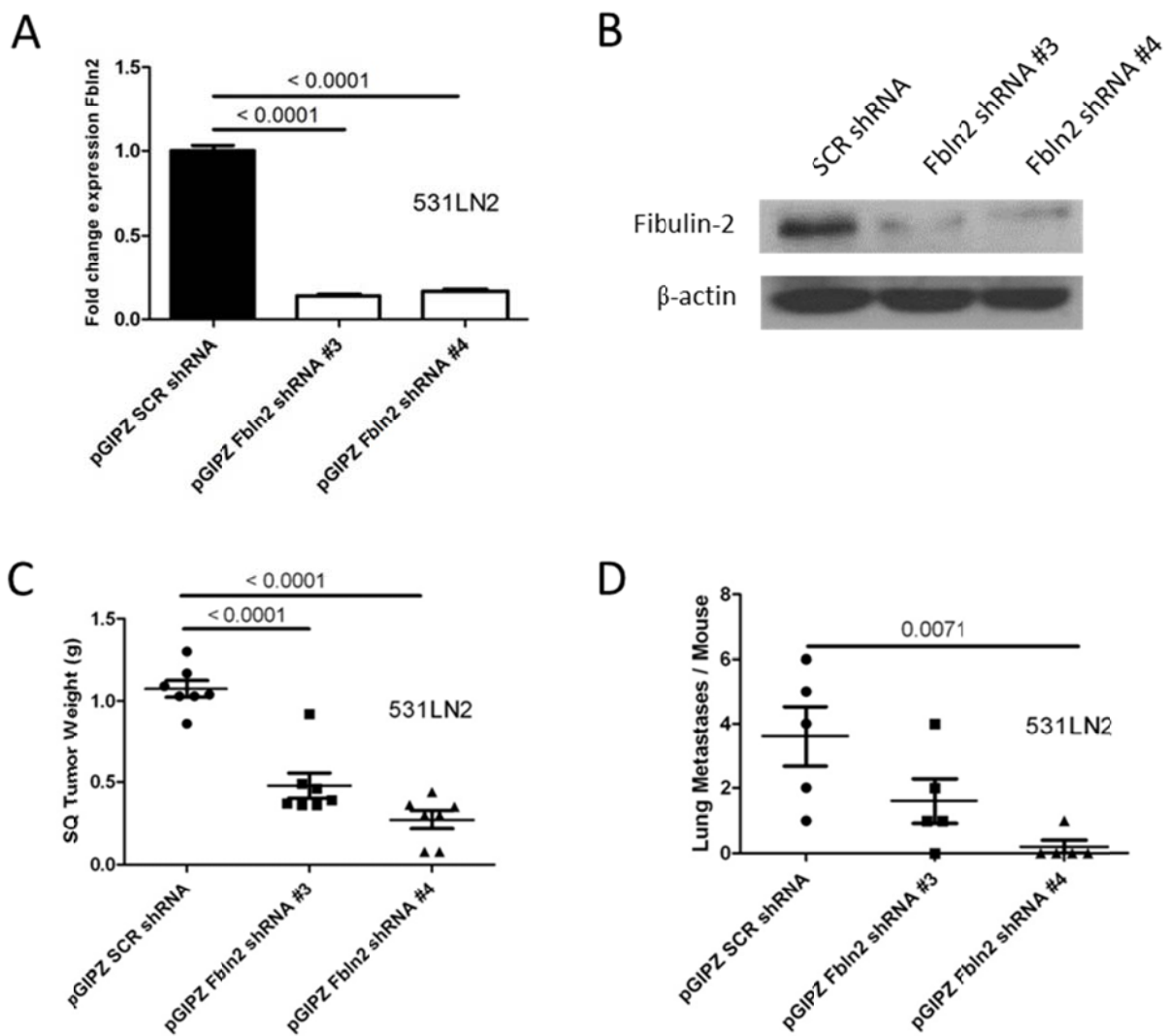


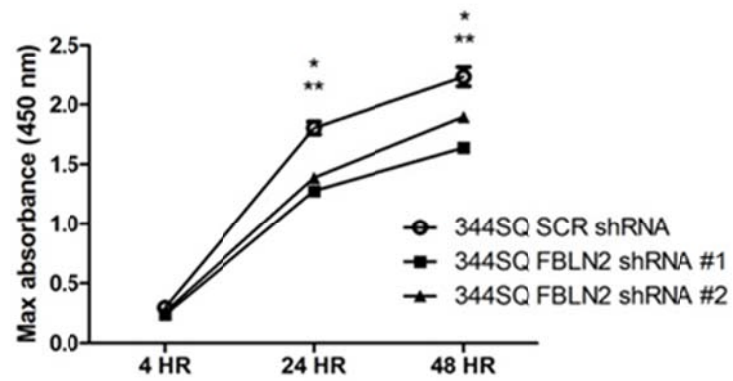
**Figure 16**

**Figure 17.** *Fibulin-2 regulates diverse biological properties of tumor cells in vitro.*

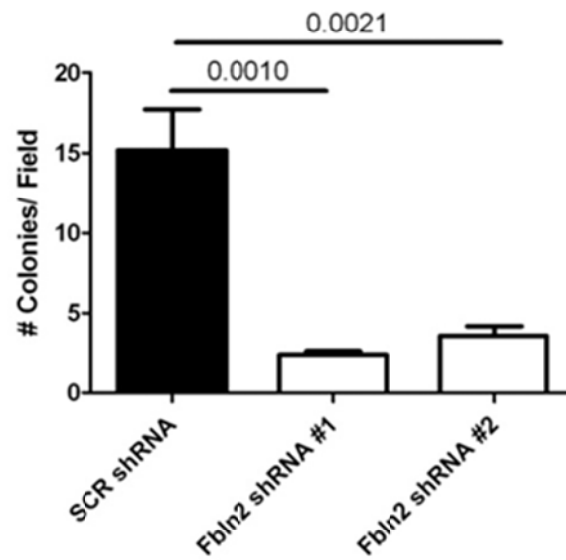
(A) MTT assays to quantify relative cell density of transfectants grown in monolayer cultures. Results expressed as mean values ( $\pm$  S.D.) at the indicated timepoints. Asterisks indicate  $P < 0.01$ , SCR shRNA versus Fbln2 shRNA. (B) Colonies grown in soft agar were counted after 21 days. Results expressed as mean values ( $\pm$  S.D.) of each cohort (bar graph). (C) Transfectants loaded into upper chambers of Boyden apparatus in the presence (+) or absence (-) of 10% serum in bottom chamber as chemo-attractant. Cells invading through Matrigel-coated filter were stained with crystal violet and quantified colorimetrically (triplicate samples). Results expressed as fold-induction by serum (bar graph).



A



B



C

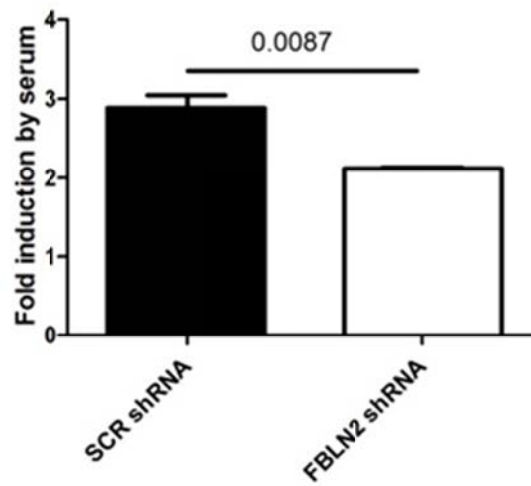
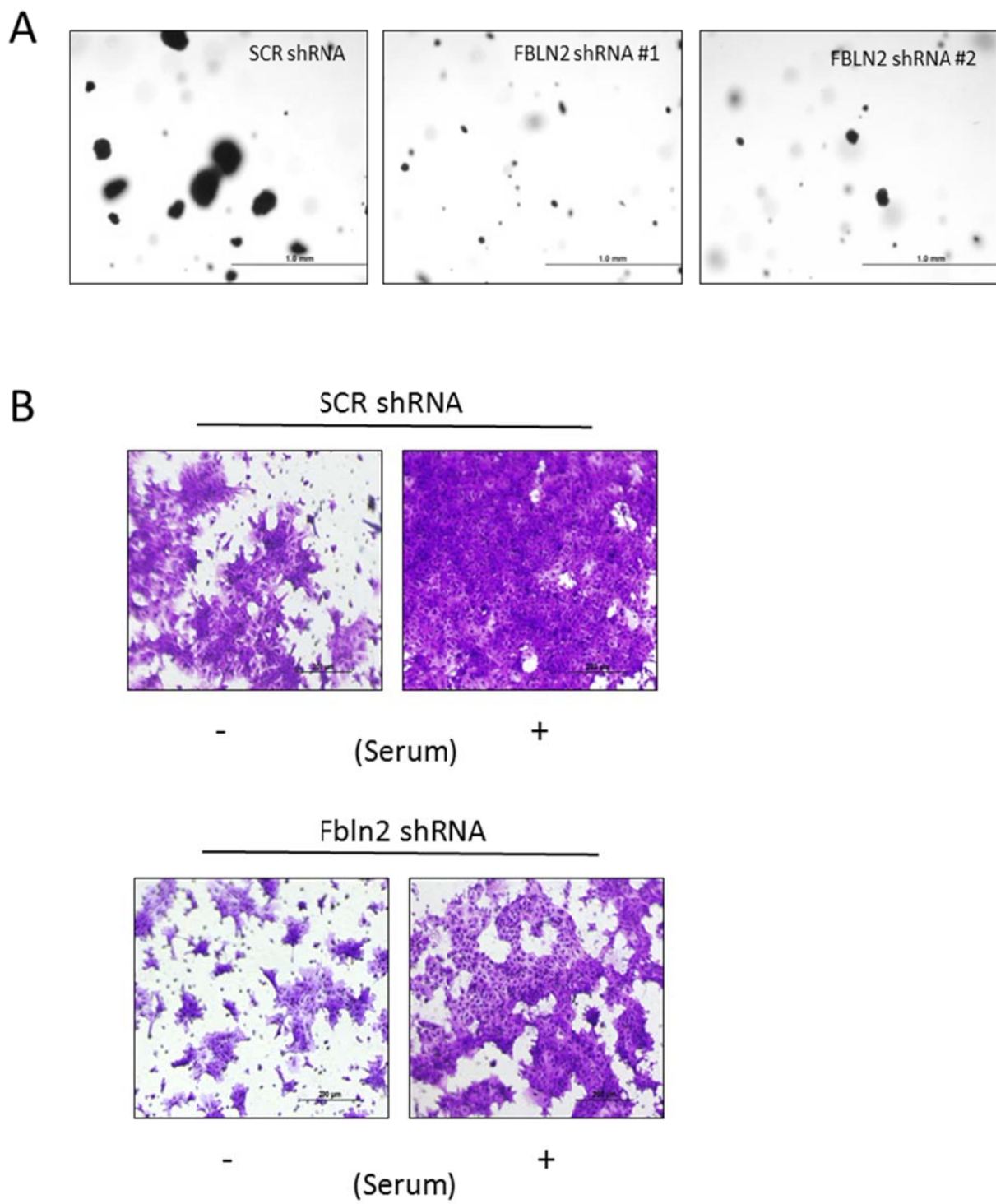


Figure 17

**Figure 18.** *Representative images from in vitro proliferation and invasion assays.*

(A) Fibulin-2-deficient (shRNA #1 and #2) and –replete (SCR shRNA) 344SQ cells were grown in soft agar for 21 days and photographed. (B) Fibulin-2-deficient (Fbln2 shRNA) and –replete (SCR shRNA) 344SQ cells were loaded into upper chambers of Boyden apparatus in the presence (+) or absence (-) of 10% serum in bottom chamber as chemo-attractant. Cells invading through Matrigel-coated filter were stained with crystal violet and photographed.



**Figure 18**

**Figure 19.** *Fibulin-2-deficient tumors have a reduction in fibrous stroma resulting in a less compact ECM.* Picosirius Red (collagen) and hematoxylin (nuclei) stained tumors (A) were converted into binary images using Image J software (B). “Particles” defined as fully enclosed areas within the binary images were counted in 48 defined areas (grids) within the interior of the tumor, excluding subcutaneous fascia, and the surface area of each particle was measured. Within a defined area, stromal collagen density correlates directly with particle numbers and indirectly with particle area. (C) Results were expressed as mean particle number per surface area and mean particle area (bar graphs). P values (t-test) are indicated.

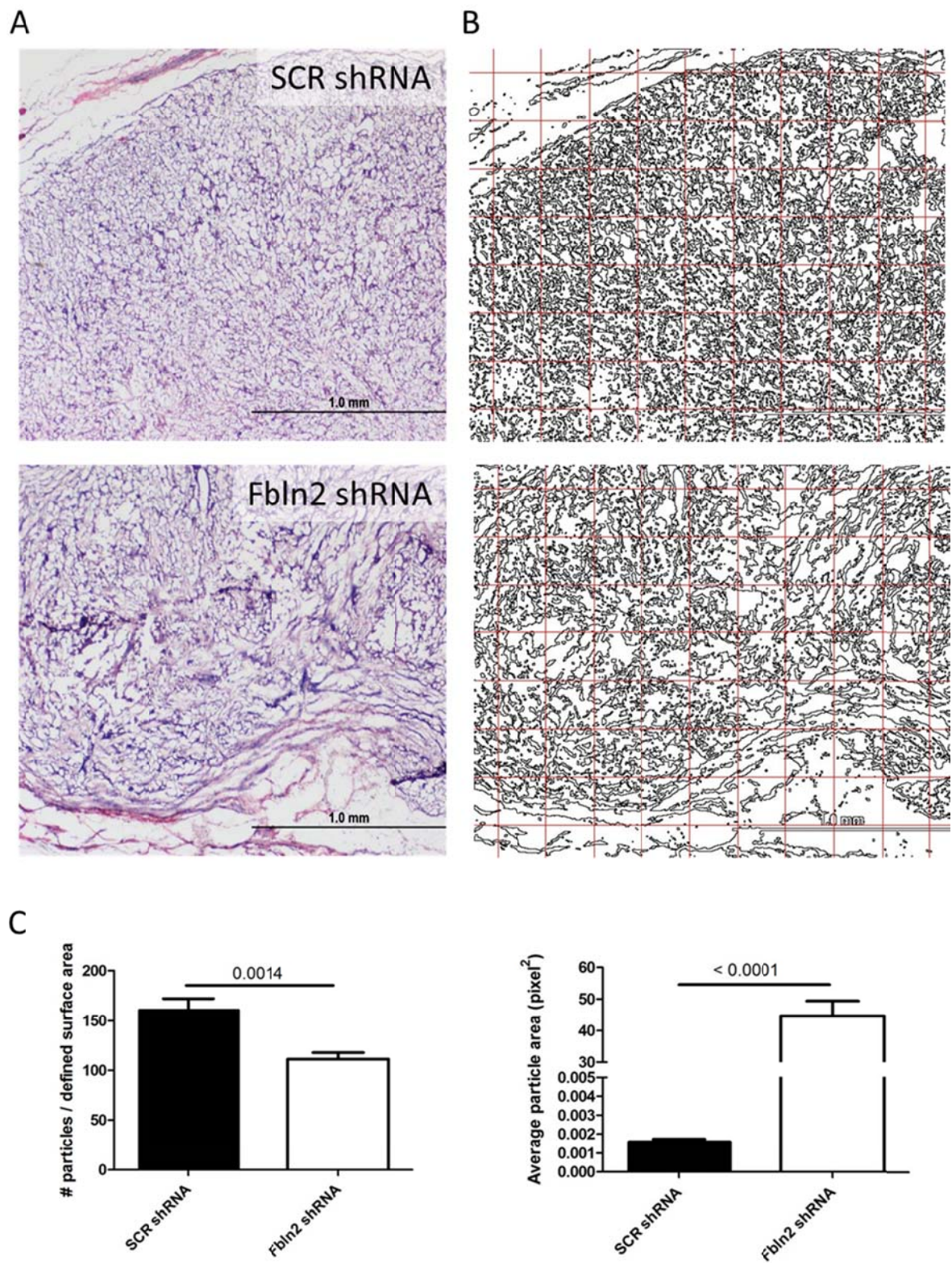


**Figure 19**

**Figure 20.** *Fibulin-2 regulates tensile properties, collagen solubility, basement membrane expression, and MMP remodeling enzymes.* (A) Compressive testing performed on punch biopsies from un-injected lungs (n=13) and orthotopic lung tumors from mice injected intra-thoracically with 344SQ cells stably transfected with Fbln2 shRNA (n=9) or SCR shRNA (n=5). Results represent mean values  $\pm$  S.D. of triplicate samples. (B) Pepsin-soluble collagen (soluble) and total collagen (total) in conditioned media samples were quantified by sircol assays and hydroxyproline assays, respectively. Results represent mean values  $\pm$  S.D. of triplicate samples. (C,D) Quantitative RT-PCR values normalized on the basis of L32 ribosomal RNA and expressed as the mean values ( $\pm$  S.D.) of quadruplicate samples relative to SCR shRNA, which was set at 1.0. (E) MMP-2 and -9 zymography (gel) of conditioned media samples from *ex vivo* lung perfusion model. Densitometric analysis of bands (bar graphs) in Fbln2 shRNA and SCR shRNA (n=3, each group). Results represent mean values  $\pm$  S.D. of triplicate samples. P-values are indicated (t-test).



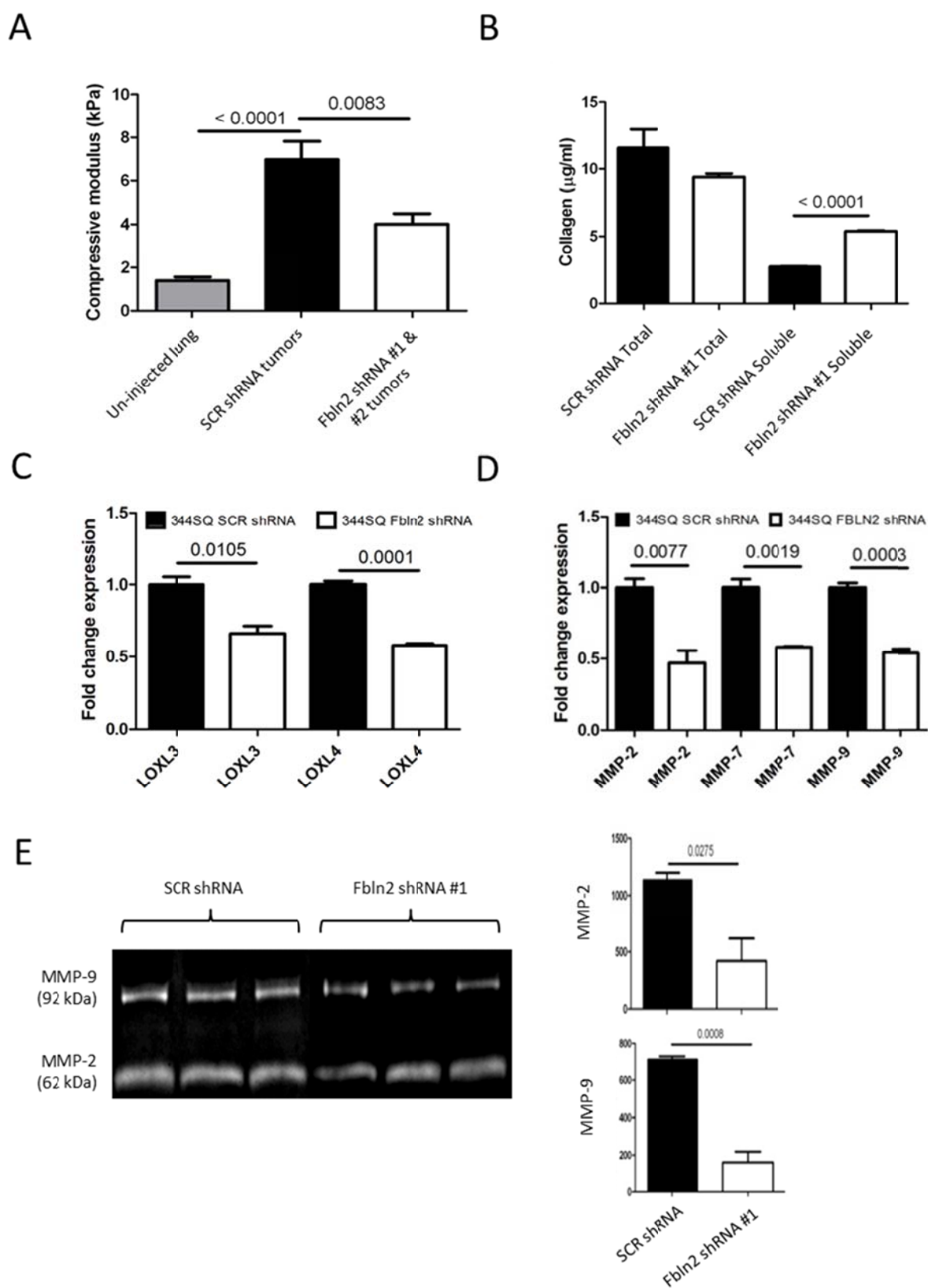


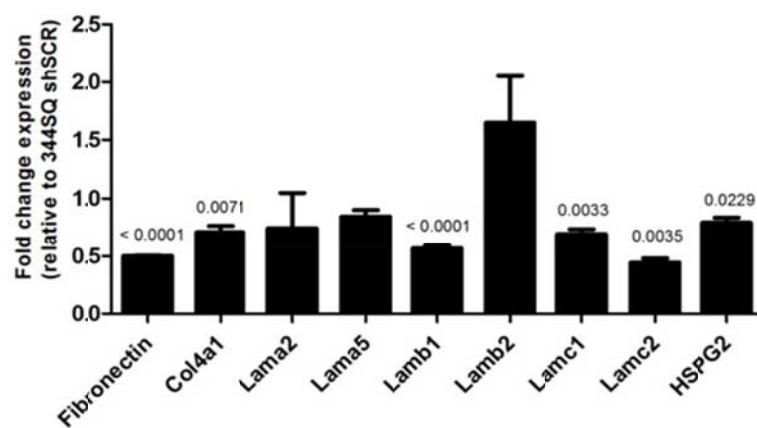
**Figure 20**

membrane components including collagen IV and laminin (Fig. 21A-B) and reduced mRNA expression of MMPs (Fig. 20D). To examine the role of lung tumor-derived fibulin-2 in a native context, we used an *ex vivo* lung perfusion model in which tissue scaffolds created by decellularization of rat lungs are injected with tumor cells through the trachea followed by continuous circulation of media through the pulmonary artery under pump pressures and conditions that maintain lung tissue architecture for up to 21 days (24). Fibulin-2-deficient or control 344SQ cells were injected through the trachea and allowed to form parenchymal lung nodules over 3 days, at which point conditioned media samples were collected and subjected to MMP zymography. Relative to scaffolds containing control tumor cells, scaffolds containing fibulin-2-deficient cells had reduced MMP-2 and MMP-9 activities (Fig. 20E). Thus, fibulin-2 was essential for tumor cells to maintain production of intrinsic matrix molecules and activated MMPs suggesting widespread effects on ECM-related tumorigenic processes (schematically illustrated in Fig. 22).



**Figure 21.** *Fibulin-2-deficient cells have reduced secretion of basement membrane components in vitro.* (A) Quantitative RT-PCR values normalized on the basis of L32 ribosomal RNA and expressed as the mean values ( $\pm$  S.D.) of quadruplicate samples relative to SCR shRNA, which was set at 1.0. (B) 344SQ cells stably transfected with Fbln2 shRNA or SCR shRNA were grown in monolayer culture and immunofluorescently stained using either an anti-pan laminin or an anti-collagen IV antibody (red). DAPI (blue).

A



B

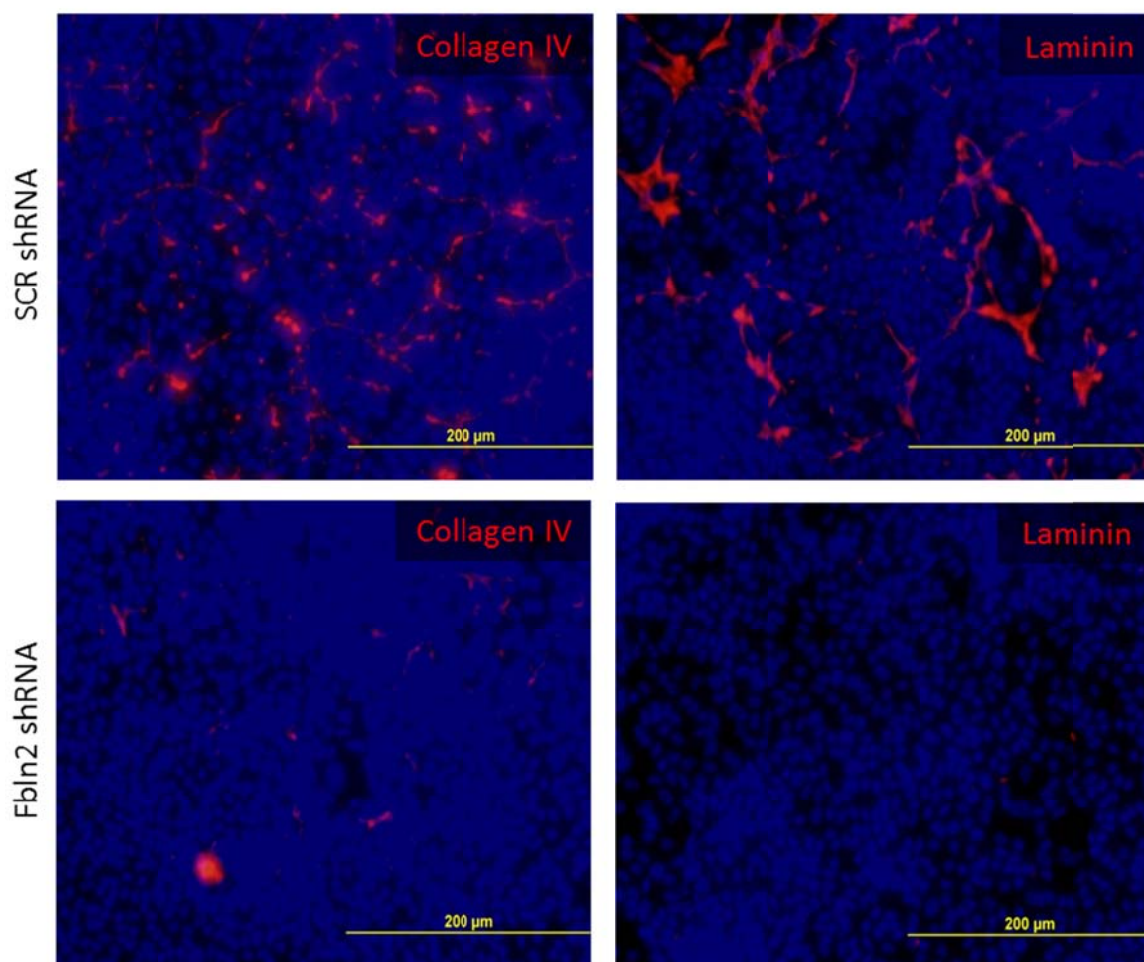


Figure 21

**Figure 22.** *Schematic illustration of Fbln2-dependent effects on tumor-associated ECM.* Tumor cell-derived Fbln2 stimulates lysyl oxidase family member transcription resulting in increased cross-linking of collagen for enhanced tumor stiffness. Fbln2 stimulates basement membrane secretion and ECM supramolecular assembly. Fbln2 enhances gelatinase MMP production leading to selective degradation of basement membrane components for increased tumor cell motility. Collectively, Fbln2 provides an intricate balance of ECM deposition, degradation, and stabilization to provide an optimal microenvironment for tumor progression and metastasis.

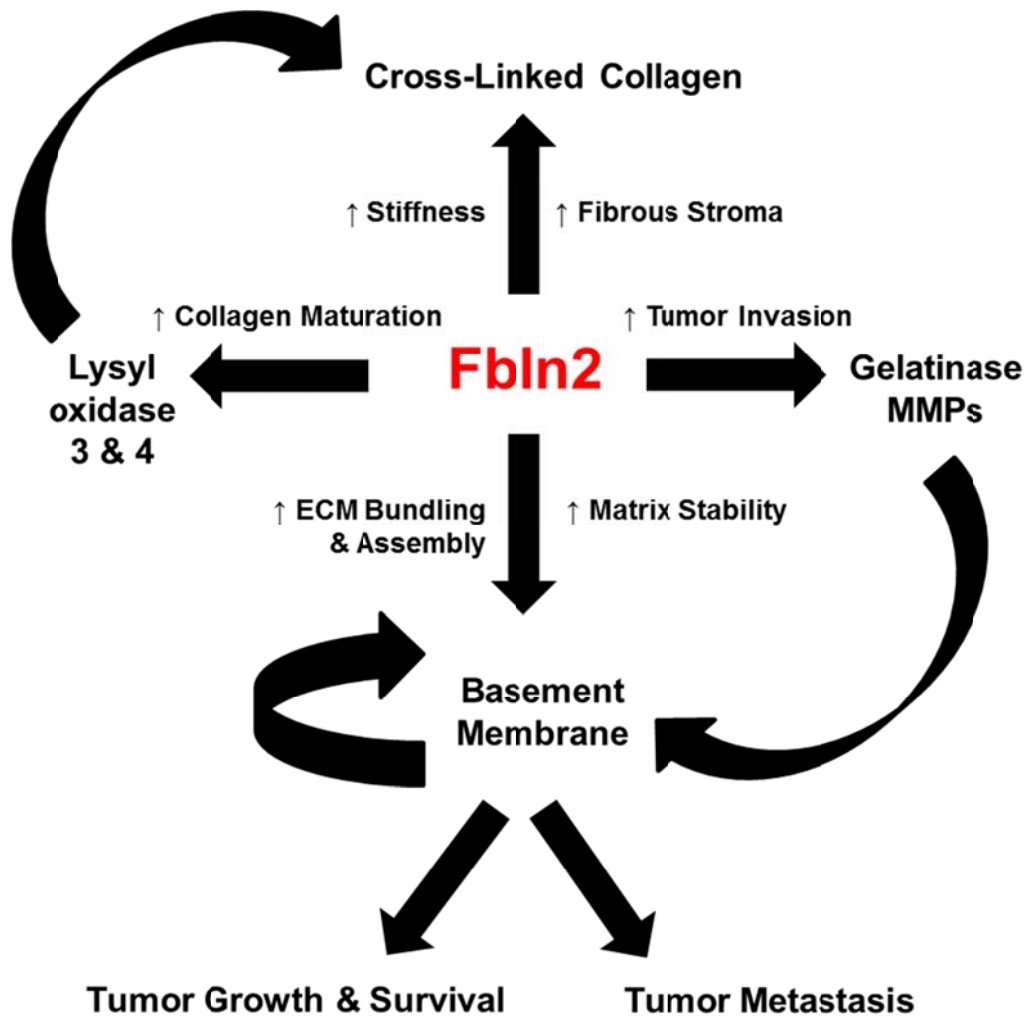


Figure 22

---

## CHAPTER 4

---

### DISCUSSION

Malignant progression of epithelial tumors is accompanied by a desmoplastic reaction and other changes in tumor ECM composition and organization that create regional heterogeneity and torsional stress (1). How tumors maintain ECM integrity in the face of dynamic biophysical forces has not been fully elucidated. Here we addressed this question in a mouse model of human lung adenocarcinoma marked by disorganized basement membranes, dense collagen networks, and increased tissue stiffness. We found that a matrix-stabilizing factor, fibulin-2, was abundant in murine and human lung adenocarcinomas, and depletion of fibulin-2 from metastasis-prone tumor cells disrupted the integrity of tumor ECM and inhibited tumor growth and metastasis. On the basis of these findings, we propose a feed-forward model in which tumor cells secrete matrix-stabilizing factors required for the assembly of an ECM that favors malignant progression (schematically illustrated in Fig. 23).

A proven oncogenic driver in epithelial cells of the lung, pancreas, and other tissue types, mutant K-ras expression is associated with an intense tumor stromal reaction (35). Moreover, fibrotic “scar” formation is a negative prognostic factor in human lung adenocarcinomas (36). Although mutant K-ras is known to up-regulate

**Figure 23.** *Schematic illustration of feed-forward model of tumor cell-derived fibulin-2 dependent matrix stabilization.* ECM stabilizing factor, Fbln2, stabilizes a mature, collagen-rich matrix derived primarily from cancer-associated fibroblasts, which stimulates tumor cells to secrete additional ECM molecules thereby engendering matrix stabilization.

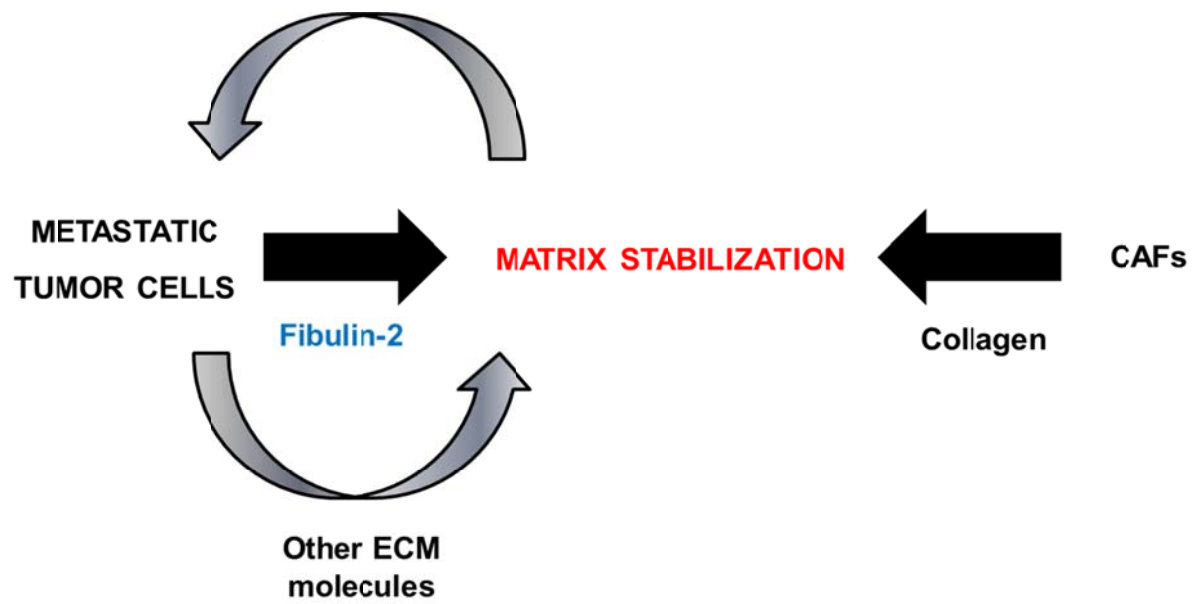


Figure 23

the expression of chemokines and cytokines that function as chemoattractants for stromal cells (35), whether CAFs contribute to mutant K-ras-driven desmoplasia has not been elucidated. Here we showed that CAFs isolated from *Kras*<sup>LA1</sup> mice produce abundant collagen type I and are deficient in collagenolytic proteases, supporting a role for CAFs in the desmoplasia associated with *Kras*-mutant tumors. CAFs are heterogeneous and originate from multiple cell types, including mesenchymal stem cells, smooth muscle cells, adipocytes, and native tissue fibroblasts (37). Thy-1<sup>pos</sup> CAFs comprised less than 1% of tumor bulk in *Kras*<sup>LA1</sup> mice, but the presence of other immunophenotypically distinct CAF populations in these mice has not been excluded. Although their intra-tumoral location in *Kras*<sup>LA1</sup> mice is unclear, CAFs are known to localize to areas of intra- and peri-tumoral fibrosis where they perform contractile functions (38), a capacity supported by evidence here that Thy-1<sup>pos</sup> CAFs have high expression of annexins and other cytoskeletal motor proteins. In addition to promoting a desmoplastic reaction, CAFs isolated from *Kras*<sup>LA1</sup> mice secrete diverse cytokines and chemokines with the potential to promote blood vessel growth, suppress anti-tumor immune responses, and enhance tumor cell invasion (9). We showed that metastatic tumor cells invaded in co-culture with CAFs and had increased adherence to collagen. Although counter-intuitive to the prevailing belief that invasive capacity is associated with a loss of adherence, increased adherence to collagen is consistent with evidence that forced expression of collagen cross-linking enzymes LOR1 or LOXL2 in tumor cells results in the formation of dense collagen fibers surrounding the tumors and the development of invasive and metastatic disease (39, 40). Thus, CAF recruitment



represents an important step in malignant progression and provides a selective advantage to *Kras*-mutant tumor cells through the secretion of factors that play multi-faceted roles in epithelial tumorigenesis (schematically illustrated in Fig. 10).

Expression profiling studies performed here revealed a complex protease signature in CAFs that included down-regulation of collagenolytic MMPs and up-regulation of multiple cathepsin family members (Ctsc, Ctsh, Ctss, Ctla, and Ctsh) in CAFs. The murine cathepsin family of proteases includes 19 members that, in epithelial tumors, originate from tumor cells and tumor-associated macrophages and, as shown here, by CAFs (41, 42). In normal tissues, cathepsins participate in intracellular turnover, immune response, and protein processing (42). In mouse models of pancreatic cancer and breast cancer, cathepsin activity is pathogenic, promoting tumor cell proliferation, angiogenesis, and apoptosis. Although mutant *K-ras* drives the expression of certain cathepsin family members in tumor cells (43), the latent *Kras*<sup>LA1</sup> allele is in a germline configuration in CAFs isolated from *Kras*<sup>LA1</sup> mice (9), arguing that mutant *K-ras* expression is not responsible for the increased cathepsin expression in CAFs. Cathepsins are synthesized as inactive zymogens that are activated by proteolytic removal of the N-terminal propeptide (42). LC-MS/MS analysis of CAFs and LFs detected these cathepsins as cleaved forms, implying that they were both over-expressed and activated. Cathepsins are involved in direct proteolytic cleavage of basement membrane components such as laminins, fibronectin, and type IV collagen (42), which, given the diminution of these ECM molecules in *Kras*<sup>LA1</sup> scaffolds, may underlie the aberrant organization of basement membranes in *Kras*<sup>LA1</sup> mice. The most prominently up-regulated cathepsin family

member in Kras<sup>LA1</sup> scaffolds was cathepsin H, which corroborates evidence that cathepsin H is abundant in lung adenocarcinomas induced by activation of a conditional Kras<sup>LA1</sup> allele (32). In that study and a separate one on human lung adenocarcinomas (44), cathepsin H was also detectable in normal lung adjacent to lung tumors, which, given our findings, may reflect peri-tumoral localization of CAFs.

A growing body of evidence suggests that intrinsic matrix proteins may function as drivers of tumorigenesis, which stands in contrast to their other role as a barrier to tumor cell invasion (45). Several recent reports have shown that tenascin C and periostin, which are matrix glycoproteins that form complexes with diverse ECM proteins, including fibronectin, and are ligands for integrins and other membrane receptors, play key roles as metastasis niche components for tumor-initiating cells (11, 46, 47). In breast tumors implanted orthotopically or arising spontaneously owing to expression of polyoma virus middle T antigen, tenascin C and periostin are expressed in tumor cells and CAFs in the metastatic niche and enhance the survival and fitness of stem-like metastasis-initiating cells through concentration of Wnt ligands (11, 46, 47). Here we showed that a matrix glycoprotein, fibulin-2, expressed in human lung adenocarcinomas and tumor cells and CAFs derived from Kras<sup>LA1</sup> mice is required for tumor growth and metastasis in mice and predicts a worse outcome in patients with lung adenocarcinoma. Although the impact of fibulin-2 on malignant progression in mice was clear, the prognostic value of fibulin-2 in human lung adenocarcinomas may reflect the known prognostic value of scar formation as opposed to a biological effect of fibulin-2 itself.

In some respects, the functional similarities between fibulin-2, tenascin C, and periostin are not surprising given that fibulin-2 forms complexes with tenascin C, and the three proteins have overlapping binding partners in the ECM (17, 48). However, several findings here suggest that fibulin-2 promotes tumorigenesis through a distinct mechanism. Unlike tenascin C and periostin, fibulin-2 was not required for lung colonization efficiency following tail vein injection, nor was it required for properties of tumor cell stem-ness on the basis of polarized sphere formation assays in 3-D cultures and expression of stem cell factors such as Nanog, Oct4, or Sox2 (data not shown). Instead, fibulin-2 exerted a pro-tumorigenic effect at the primary site, where it stabilized ECM organization and structure. Extending the analogy of fibulin-2-deficient tumors to *Fbln2*-null mice subjected to myocardial infarction (21), myocytes in damaged cardiac tissues and cells within the stroma of epithelial tumors are both under chronic hypoxic stress and respond to tissue injury by secreting intrinsic matrix proteins and matrix cross-linking enzymes (49, 50). Findings presented here suggest that stress-induced matrix secretion is impaired in fibulin-2-deficient tumors. The ECM of fibulin-2-depleted tumors was not only poorly organized, a predicted phenotype of fibulin-2 deficiency on the basis of fibulin-2's capacity to form bridges between supra-molecular structures (20), but it was also deficient in diverse intrinsic matrix proteins. Although this deficiency could be related in part to rapid catabolism of damaged and poorly organized matrix proteins, we showed that the expression of diverse ECM proteins is down-regulated in fibulin-2-depleted tumor cells. On the basis of these findings, we propose a feed-forward model in which epithelial carcinoma cells secrete fibulin-2, which leads to the

assembly of a matrix with structure and organization that favors tumor growth and metastasis.

## **GRANT SUPPORT**

This study was supported in part by R01 CA157450 (J.M.K.), The Elza and Ina Shackelford-Freeman Lung Cancer Research Professorship (J.M.K.), and U01CA141550 (S.H.).

## REFERENCES

1. Nelson, C. M., and M. J. Bissell. 2006. Of extracellular matrix, scaffolds, and signaling: tissue architecture regulates development, homeostasis, and cancer. *Annu Rev Cell Dev Biol* 22:287-309.
2. Cox, T. R., and J. T. Erler. 2011. Remodeling and homeostasis of the extracellular matrix: implications for fibrotic diseases and cancer. *Dis Model Mech* 4:165-178.
3. Levental, K. R., H. Yu, L. Kass, J. N. Lakins, M. Egeblad, J. T. Erler, S. F. Fong, K. Csiszar, A. Giaccia, W. Weninger, M. Yamauchi, D. L. Gasser, and V. M. Weaver. 2009. Matrix crosslinking forces tumor progression by enhancing integrin signaling. *Cell* 139:891-906.
4. Ebihara, T., N. Venkatesan, R. Tanaka, and M. S. Ludwig. 2000. Changes in extracellular matrix and tissue viscoelasticity in bleomycin-induced lung fibrosis. Temporal aspects. *Am J Respir Crit Care Med* 162:1569-1576.
5. Paszek, M. J., N. Zahir, K. R. Johnson, J. N. Lakins, G. I. Rozenberg, A. Gefen, C. A. Reinhart-King, S. S. Margulies, M. Dembo, D. Boettiger, D. A. Hammer, and V. M. Weaver. 2005. Tensional homeostasis and the malignant phenotype. *Cancer Cell* 8:241-254.
6. Ramaswamy, S., K. N. Ross, E. S. Lander, and T. R. Golub. 2003. A molecular signature of metastasis in primary solid tumors. *Nat Genet* 33:49-54.
7. Olson, M. F., and E. Sahai. 2009. The actin cytoskeleton in cancer cell motility. *Clin Exp Metastasis* 26:273-287.

8. Johnson, L., K. Mercer, D. Greenbaum, R. T. Bronson, D. Crowley, D. A. Tuveson, and T. Jacks. 2001. Somatic activation of the K-ras oncogene causes early onset lung cancer in mice. *Nature* 410:1111-1116.
9. Roybal, J. D., Y. Zang, Y. H. Ahn, Y. Yang, D. L. Gibbons, B. N. Baird, C. Alvarez, N. Thilaganathan, D. D. Liu, P. Saintigny, J. V. Heymach, C. J. Creighton, and J. M. Kurie. miR-200 Inhibits lung adenocarcinoma cell invasion and metastasis by targeting Flt1/VEGFR1. *Mol Cancer Res* 9:25-35.
10. Egeblad, M., L. E. Littlepage, and Z. Werb. 2005. The fibroblastic coconspirator in cancer progression. *Cold Spring Harb Symp Quant Biol* 70:383-388.
11. Oskarsson, T., S. Acharyya, X. H. Zhang, S. Vanharanta, S. F. Tavazoie, P. G. Morris, R. J. Downey, K. Manova-Todorova, E. Brogi, and J. Massague. Breast cancer cells produce tenascin C as a metastatic niche component to colonize the lungs. *Nat Med* 17:867-874.
12. Zheng, S., A. K. El-Naggar, E. S. Kim, J. M. Kurie, and G. Lozano. 2007. A genetic mouse model for metastatic lung cancer with gender differences in survival. *Oncogene* 26:6896-6904.
13. Schliekelman, M. J., D. L. Gibbons, V. M. Faca, C. J. Creighton, Z. H. Rizvi, Q. Zhang, C. H. Wong, H. Wang, C. Ungewiss, Y. H. Ahn, D. H. Shin, J. M. Kurie, and S. M. Hanash. Targets of the tumor suppressor miR-200 in regulation of the epithelial-mesenchymal transition in cancer. *Cancer Res* 71:7670-7682.

14. de Vega, S., T. Iwamoto, and Y. Yamada. 2009. Fibulins: multiple roles in matrix structures and tissue functions. *Cell Mol Life Sci* 66:1890-1902.
15. Moll, F., D. Katsaros, G. Lazennec, N. Hellio, P. Roger, P. L. Giacalone, D. Chalbos, T. Maudelonde, H. Rochefort, and P. Pujol. 2002. Estrogen induction and overexpression of fibulin-1C mRNA in ovarian cancer cells. *Oncogene* 21:1097-1107.
16. Qing, J., V. M. Maher, H. Tran, W. S. Argraves, R. W. Dunstan, and J. J. McCormick. 1997. Suppression of anchorage-independent growth and matrigel invasion and delayed tumor formation by elevated expression of fibulin-1D in human fibrosarcoma-derived cell lines. *Oncogene* 15:2159-2168.
17. Argraves, W. S., L. M. Greene, M. A. Cooley, and W. M. Gallagher. 2003. Fibulins: physiological and disease perspectives. *EMBO Rep* 4:1127-1131.
18. Timpl, R., T. Sasaki, G. Kostka, and M. L. Chu. 2003. Fibulins: a versatile family of extracellular matrix proteins. *Nat Rev Mol Cell Biol* 4:479-489.
19. Pan, T. C., T. Sasaki, R. Z. Zhang, R. Fassler, R. Timpl, and M. L. Chu. 1993. Structure and expression of fibulin-2, a novel extracellular matrix protein with multiple EGF-like repeats and consensus motifs for calcium binding. *J Cell Biol* 123:1269-1277.
20. Sasaki, T., K. Mann, H. Wiedemann, W. Gohring, A. Lustig, J. Engel, M. L. Chu, and R. Timpl. 1997. Dimer model for the microfibrillar protein fibulin-2 and identification of the connecting disulfide bridge. *EMBO J* 16:3035-3043.

21. Tsuda, T., J. Wu, E. Gao, J. Joyce, D. Markova, H. Dong, Y. Liu, H. Zhang, Y. Zou, F. Gao, T. Miller, W. Koch, X. Ma, and M. L. Chu. 2012. Loss of fibulin-2 protects against progressive ventricular dysfunction after myocardial infarction. *J Mol Cell Cardiol* 52:273-282.
22. Gibbons, D. L., W. Lin, C. J. Creighton, Z. H. Rizvi, P. A. Gregory, G. J. Goodall, N. Thilaganathan, L. Du, Y. Zhang, A. Pertsemlidis, and J. M. Kurie. 2009. Contextual extracellular cues promote tumor cell EMT and metastasis by regulating miR-200 family expression. *Genes Dev* 23:2140-2151.
23. Jacoby, J. J., B. Erez, M. V. Korshunova, R. R. Williams, K. Furutani, O. Takahashi, L. Kirkpatrick, S. M. Lippman, G. Powis, M. S. O'Reilly, and R. S. Herbst. 2010. Treatment with HIF-1alpha antagonist PX-478 inhibits progression and spread of orthotopic human small cell lung cancer and lung adenocarcinoma in mice. *J Thorac Oncol* 5:940-949.
24. Mishra, D. K., M. J. Thrall, B. N. Baird, H. C. Ott, S. H. Blackmon, J. M. Kurie, and M. P. Kim. Human lung cancer cells grown on acellular rat lung matrix create perfusable tumor nodules. *Ann Thorac Surg* 93:1075-1081.
25. Ngoka, L. C. 2008. Sample prep for proteomics of breast cancer: proteomics and gene ontology reveal dramatic differences in protein solubilization preferences of radioimmunoprecipitation assay and urea lysis buffers. *Proteome Sci* 6:30.
26. Dennis, G., Jr., B. T. Sherman, D. A. Hosack, J. Yang, W. Gao, H. C. Lane, and R. A. Lempicki. 2003. DAVID: Database for Annotation, Visualization, and Integrated Discovery. *Genome Biol* 4:P3.



27. Hagood, J. S., P. Prabhakaran, P. Kumbala, L. Salazar, M. W. MacEwen, T. H. Barker, L. A. Ortiz, T. Schoeb, G. P. Siegal, C. B. Alexander, A. Pardo, and M. Selman. 2005. Loss of fibroblast Thy-1 expression correlates with lung fibrogenesis. *Am J Pathol* 167:365-379.
28. Yi, C. H., D. J. Smith, W. W. West, and M. A. Hollingsworth. 2007. Loss of fibulin-2 expression is associated with breast cancer progression. *Am J Pathol* 170:1535-1545.
29. Beacham, D. A., M. D. Amatangelo, and E. Cukierman. 2007. Preparation of extracellular matrices produced by cultured and primary fibroblasts. *Curr Protoc Cell Biol* Chapter 10:Unit 10 19.
30. Behrens, C., H. Y. Lin, J. J. Lee, M. G. Raso, W. K. Hong, Wistuba, II, and R. Lotan. 2008. Immunohistochemical expression of basic fibroblast growth factor and fibroblast growth factor receptors 1 and 2 in the pathogenesis of lung cancer. *Clin Cancer Res* 14:6014-6022.
31. Vargova, V., M. Pytliak, and V. Mechirova. 2012. Matrix metalloproteinases. *EXS* 103:1-33.
32. Grimm, J., D. G. Kirsch, S. D. Windsor, C. F. Kim, P. M. Santiago, V. Ntziachristos, T. Jacks, and R. Weissleder. 2005. Use of gene expression profiling to direct in vivo molecular imaging of lung cancer. *Proc Natl Acad Sci U S A* 102:14404-14409.
33. Wilson, W. R., and M. P. Hay. 2011. Targeting hypoxia in cancer therapy. *Nat Rev Cancer* 11:393-410.

34. Sasaki, T., H. Wiedemann, M. Matzner, M. L. Chu, and R. Timpl. 1996. Expression of fibulin-2 by fibroblasts and deposition with fibronectin into a fibrillar matrix. *J Cell Sci* 109 ( Pt 12):2895-2904.
35. Neesse, A., P. Michl, K. K. Frese, C. Feig, N. Cook, M. A. Jacobetz, M. P. Lolkema, M. Buchholz, K. P. Olive, T. M. Gress, and D. A. Tuveson. 2011. Stromal biology and therapy in pancreatic cancer. *Gut* 60:861-868.
36. Maeshima, A. M., T. Niki, A. Maeshima, T. Yamada, H. Kondo, and Y. Matsuno. 2002. Modified scar grade: a prognostic indicator in small peripheral lung adenocarcinoma. *Cancer* 95:2546-2554.
37. Kalluri, R., and M. Zeisberg. 2006. Fibroblasts in cancer. *Nat Rev Cancer* 6:392-401.
38. Sugimoto, H., T. M. Mundel, M. W. Kieran, and R. Kalluri. 2006. Identification of fibroblast heterogeneity in the tumor microenvironment. *Cancer Biol Ther* 5:1640-1646.
39. Akiri, G., E. Sabo, H. Dafni, Z. Vadasz, Y. Kartvelishvily, N. Gan, O. Kessler, T. Cohen, M. Resnick, M. Neeman, and G. Neufeld. 2003. Lysyl oxidase-related protein-1 promotes tumor fibrosis and tumor progression in vivo. *Cancer Res* 63:1657-1666.
40. Peng, L., Y. L. Ran, H. Hu, L. Yu, Q. Liu, Z. Zhou, Y. M. Sun, L. C. Sun, J. Pan, L. X. Sun, P. Zhao, and Z. H. Yang. 2009. Secreted LOXL2 is a novel therapeutic target that promotes gastric cancer metastasis via the Src/FAK pathway. *Carcinogenesis* 30:1660-1669.

41. Shree, T., O. C. Olson, B. T. Elie, J. C. Kester, A. L. Garfall, K. Simpson, K. M. Bell-McGuinn, E. C. Zabor, E. Brogi, and J. A. Joyce. 2011. Macrophages and cathepsin proteases blunt chemotherapeutic response in breast cancer. *Genes Dev* 25:2465-2479.
42. Vasiljeva, O., and B. Turk. 2008. Dual contrasting roles of cysteine cathepsins in cancer progression: apoptosis versus tumour invasion. *Biochimie* 90:380-386.
43. Cavallo-Medved, D., J. Dosesu, B. E. Linebaugh, M. Sameni, D. Rudy, and B. F. Sloane. 2003. Mutant K-ras regulates cathepsin B localization on the surface of human colorectal carcinoma cells. *Neoplasia* 5:507-519.
44. Schweiger, A., A. Staib, B. Werle, M. Krasovec, T. T. Lah, W. Ebert, V. Turk, and J. Kos. 2000. Cysteine proteinase cathepsin H in tumours and sera of lung cancer patients: relation to prognosis and cigarette smoking. *Br J Cancer* 82:782-788.
45. Rowe, R. G., and S. J. Weiss. 2009. Navigating ECM barriers at the invasive front: the cancer cell-stroma interface. *Annu Rev Cell Dev Biol* 25:567-595.
46. Malanchi, I., A. Santamaria-Martinez, E. Susanto, H. Peng, H. A. Lehr, J. F. Delaloye, and J. Huelsken. 2012. Interactions between cancer stem cells and their niche govern metastatic colonization. *Nature* 481:85-89.
47. O'Connell, J. T., H. Sugimoto, V. G. Cooke, B. A. MacDonald, A. I. Mehta, V. S. LeBleu, R. Dewar, R. M. Rocha, R. R. Brentani, M. B. Resnick, E. G. Neilson, M. Zeisberg, and R. Kalluri. 2011. VEGF-A and Tenascin-C

produced by S100A4+ stromal cells are important for metastatic colonization.  
Proc Natl Acad Sci U S A 108:16002-16007.

48. Kusubata, M., A. Hirota, T. Ebihara, K. Kuwaba, Y. Matsubara, T. Sasaki, M. Kusakabe, T. Tsukada, S. Irie, and Y. Koyama. 1999. Spatiotemporal changes of fibronectin, tenascin-C, fibulin-1, and fibulin-2 in the skin during the development of chronic contact dermatitis. J Invest Dermatol 113:906-912.
49. Erler, J. T., and A. J. Giaccia. 2006. Lysyl oxidase mediates hypoxic control of metastasis. Cancer Res 66:10238-10241.
50. Jean, C., P. Gravelle, J. J. Fournie, and G. Laurent. 2011. Influence of stress on extracellular matrix and integrin biology. Oncogene 30:2697-2706.

## CURRICULUM VITAE

**Name** Brandi N. Baird  
**Date of Birth** November 5, 1981  
**Citizenship** United States of America  
**Current Status** \_\_\_\_\_

### Ph.D. Graduate Student (2012)

UT MD Anderson Cancer Center  
1515 Holcombe Blvd.  
Houston, Tx 77030  
Phone: (713) 745-1504  
E-mail: [bnbaird@mdanderson.org](mailto:bnbaird@mdanderson.org)

Cumulative G.P.A.: 3.9

### Ph.D. Thesis Title & Advisor

“Fibulin-2 stabilizes tumor extracellular matrix and drives malignant progression of lung adenocarcinoma”.

Supervisory Professor: Jonathan M. Kurie, M.D., Professor, UT MD Anderson Cancer Center, E-mail: [jkurie@mdanderson.org](mailto:jkurie@mdanderson.org)

### Education

 \_\_\_\_\_

#### M.S. Biochemistry & Molecular Biology (2006)

Graduate School of  
Biomedical Sciences  
University of Texas Health  
Science Center-Houston  
P.O. Box 20334, Houston,  
Texas 77225

#### M.S. Thesis Title & Advisor

“The Characterization of IL-19 and TNF- $\alpha$  in Adenosine Mediated Lung Injury”

Supervisory Professor: Michael R. Blackburn, Ph.D., Professor and Director, Biochemistry and Molecular Biology Graduate Program, UT Medical School, E-mail: [Michael.R.Blackburn@uth.tmc.edu](mailto:Michael.R.Blackburn@uth.tmc.edu)

#### B.S. Biology, Magna Cum Laude (2004)

Stephen F. Austin State University  
1936 North Street, Nacogdoches, Texas 75961  
Undergraduate Research: Dr. Wayne Boring (Chemist), Welch Scholarship

## Honors & Awards

---

2005

- UT Health Science Center Golf Classic Scholarship

2008

- William A. and Madelyn Welder Smith Fellowship in Stem Cell Research
- American Association for the Advancement of Science
- Poster Competition Award FASEB: Lung Epithelium in Development and Disease

- American Legion Auxiliary Fellowship

2009

- Renewal William A. and Madelyn Welder Smith Fellowship in Stem Cell Research
- American Legion Auxiliary Fellowship Renewal

2010

- American Legion Auxiliary Fellowship Renewal

## Expertise, Competencies, & Interests

---

### Expertise:

extracellular matrix, lung cancer tumorigenesis and metastasis, microenvironment, stem cell biology, lung scaffolds, tumor microenvironment, flow cytometry, prospective isolation strategies, collagen metabolism, small animal surgeries, proteomic profiling, pathology, histology

### Competencies:

oral and written presentation skills in conveying novel scientific research to diverse audiences, project design and managements, statistical analyses and assessment of scientific data, advanced computer skills, leadership experience

### Interests:

metastatic niche, matrisome, biomechanical and biophysical interactions, tumor-stromal microenvironment, adult lung stem cells, basic lung physiology, tissue regeneration; cellular based therapies, translational and clinical research

## Technical Skills

---

Isolation and characterization of stem cells and stromal cell compartments from adult normal lung and tumorigenic tissues; multi-color flow cytometric analysis and fluorescent-activated cell sorting; *in vitro* clonogenic assays; *in vivo* cellular transplant models (mice); use of monoclonal reagents to phenotypically and functionally dissect tissues to identify stem cell populations; cell lineage depletion;

enzyme replacement therapy; lung cellularity: immunocytochemistry and immunofluorescence; histological analyses of lung necropsies: immunohistochemistry; *in vitro* tissue culture; isolation and propagation of primary and immortalized cells; expression analyses through real time rtPCR and microarray; protein analyses through Western blot and ELISA; fluorescence and confocal microscopy; cloning; gene therapy techniques including adenoviral transfection and infection; viral vector design, construction and generation; pathologic examination of diseased lungs and brain tumors

## Certifications

---

- *Animal Research Training Course*- Univ. of Tx Center for Laboratory Animal Medicine and Care (2004)
- *The Design and Management of Clinical Trials*- Certification Program: The Univ. of Tx & M.D. Anderson Cancer Center (2007)

## Teaching Experience

---

Private and group session tutoring in undergraduate biology and chemistry

## Professional Development

---

2006

- BioHouston Texas Life Science Conference: Breakthrough Research, Commercial Success
- Univ. of Tx & M.D. Anderson 59<sup>th</sup> Annual Symposium on Cancer Research: Stem Cells in Cancer and Regenerative Medicine

2008

- U.T. M.D. Anderson 61<sup>st</sup> Annual Symposium on Cancer Research: Systems Biology of Cancer
- Cardiovascular Regeneration Seminar Series and Workshop- UT School of Health Information Sciences and Texas Heart Institute

## Professional Presentations

---

2005-2006

- "IL-19 and TNF- $\alpha$  in the Lungs of *ADA*<sup>-/-</sup> Mice"- poster competitions, Univ.

of Tx BMB department, GSEC, & IMM

2008

- “Isolation of Stem Cells in the Adult Mouse Lung: Keys to Developing Regenerative Therapies for Intractable Lung Disease”- Leaders of Tomorrow Event
- “Identification and Characterization of Prospectively Isolated Candidate Stem/Progenitor Cells in the Adult Mouse Lung”- FASEB Summer Research Conference: Lung Epithelium in Development and Disease
- “Respiratory Stem Cells in Regeneration of the Adult Mouse Lung: Will the real stem cell please stand up?”- IMM Centre for Stem Cell Research
- “Identification and Characterization of Prospectively Isolated Candidate Stem/Progenitor Cells in the Adult Mouse Lung”- UTHSC Research Day

2009

- “Identification and Characterization of Prospectively Isolated Candidate Stem/Progenitor Cells in the Adult Mouse Lung”- Keystone Symposia: Fibrosis- Short Talk
- “Identification and Characterization of Prospectively Isolated

Stem/Progenitor Cells in the Adult Mouse Lung”- Scientific Advisory Board

- “Competitiveness Initiative: A Student’s Prospective”- UT Board of Regents meeting, Austin, Tx

2011

- “The Magic is in the Matrix: Using Nature’s Architectural Platform to Treat Lung Cancer Tumorigenesis and Metastasis”- Keystone Symposia: Extracellular Matrix and Cardiovascular Remodeling
- “The Magic is in the Matrix: Using Nature’s Architectural Platform to Treat Lung Cancer Tumorigenesis and Metastasis”- Keystone Symposia: Lung Development and Repair
- “De-cellularized Rat Matrix Selects Highly Invasive Human A549 Lung Cancer Cells”- AACR: Tumor Microenvironment Complexity: Emerging Roles in Cancer Therapy

2012

- “A tumor ECM that is collagen-rich owing to CAFs and requires Fbln2 to promote malignant progression”- Gordon research conference: Signaling by Adhesion Receptors



## Peer-reviewed Scientific Publications

---

1. "Fibulin-2 stabilizes tumor extracellular matrix and drives malignant progression of lung adenocarcinoma." **Baird BN**, Schliekelman MJ, Roybal JD, Chen Y, Gill BJ, Mishra DK, Erez B, O'Reilly MS, Yang Y, Ahn YH, Patel M, Liu X, Thilaganathan N, Larina IV, Dickinson ME, West JL, Gibbons DL, Liu D, Kim MP, Hicks JM, Wistuba II, Hanash SM, Kurie JM. *The Journal of Clinical Investigation*. (Currently under review).
2. "Human Lung Cancer Cell Lines Grown on Decellularized Rat Matrices Mimic Human Lung Cancer Histopathology." Mishra D, Thrall MJ, **Baird BN**, Ott HC, Blackmon SH, Kurie JM, Kim MP. *The Annals of Thoracic Surgery*. 2012.
3. "miR-200 Inhibits lung adenocarcinoma cell invasion and metastasis by targeting Flt1/VEGFR1." Roybal JD, Zang Y, Ahn YH, Yang Y, Gibbons DL, **Baird BN**, Alvarez C, Thilaganathan N, Liu DD, Saintigny P, Heymach JV, Creighton CJ, Kurie JM. *Mol. Cancer Res*. 2011.
4. "Endogenous fibroblastic progenitor cells in the adult mouse lung are highly enriched in the Sca-1 positive cell fraction." McQualter JL, Brouard N, Williams B, **Baird BN**, Sims-Lucas S, Yuen K, Nilsson SK, Simmons PJ, Bertoncello I. *Stem Cells*. 2009.

## Contributions to Univ. of Tx Graduate School

---

Biochemistry and Molecular Biology Program Student Liaison/Representative, Biochemistry and Molecular Biology Program Steering Committee, Graduate Student Association, International Student Buddy, Volunteer for the National Youth, Leadership Forum high school student visit, Student Recruitment Weekend Ringleader (two years), Visitation Weekend Student Escort, Multiple Tier I Course, Review Sessions, Evening of Discovery Philanthropic Event, Lunch Meetings with members of the Texas Legislative Staff, Meeting with Houston City Council Member, Mrs. Pam Holm, Presentation to prospective UT Development Board, Presentation for UT-Health Science Center Development Board: GSBS' award-winning students of the day, Presentation for UT Board of Regents in Austin, TX

## Professional Affiliations

---

- Member AAAS
- BioHouston Steering Committee
- Rice Alliance
- Committee on the Status of Women

## Other Information

---

First generation college student

### Governor Rick Perry's tour of the IMM (*Distinctions*, Dec. 2007)



Texas Gov. Rick Perry, second from left, listens to graduate student Brandi Baird, foreground, as she explains some of the work she does in the lab of Paul Simmons, Ph.D., professor and director of the Center for Stem Cell Research at the Brown Foundation Institute of Molecular Medicine for the Prevention of Human Diseases (IMM), far right. David Haviland, Ph.D., assistant professor, far right, and C. Thomas Caskey, M.D., Ph.D., director and chief executive officer of the IMM, second from right, participated in the governor's tour on Nov. 1 when Perry spoke at the Texas Life Science Conference at the IMM. *Photo by John Everett*

### Philanthropist Harry Bovay Honored During Boy Scout Tour at IMM (*Distinctions*, Aug. 2008)



From left, Brandi Baird, a graduate student working at the IMM; David Haviland, Ph.D., assistant professor at the IMM; Bovay; Irma Gigli, Ph.D., deputy director of the IMM; and Eva Zsigmond, Ph.D., IMM assistant professor, hosted 22 students from the high school for a morning of education in research at the IMM. The event included hands-on presentations in the flow cytometry and fluorescent microscopy labs. Baird, an alumna of DeBakey High School, spoke to the students about her goals that led to her current research at the IMM. Gigli and Haviland also are on faculty at the Graduate School of Biomedical Sciences.